This is a preprint, the final version is subject to change, of the American Mineralogist (MSA)
Cite as Authors (Year) Title. American Mineralogist, in press.
(DOI will not work until issue is live.) DOI: http://dx.doi.org/10.2138/am.2013.4265

4265 Rivision4

Mid- and far-infrared spectra of synthetic $CaMg_2(Al_{4-x}Ga_x)(Si_{1-y}Ge_y)O_{10}(OH,OD)_2$-clintonite: Characterization and assignment of the $Ca\text{-}O_{inner}$ and $Ca\text{-}O_{outer}$ stretching bands

KIYOTAKA ISHIDA*

*Department of Environmental Changes, Graduate School of Social and Cultural Studies, Kyushu University, 744 Motooka, Nishi-ku, Fukuoka 819-0395, Japan

Keywords: Rietveld refinement, far infrared spectra, synthetic clintonite, $Ca\text{-}O_{inner}$ stretching band, $Ca\text{-}O_{outer}$ stretching band

Running title: MIR AND FIR FOR CLINTONITE

Written with Microsoft Office Word 2007

*: e-mail: kiyota@scs.kyushu-u.ac.jp

ABSTRACT

X-ray diffraction Rietveld structure refinement and mid- and far-infrared spectral studies have been done on Ga-for-Al and Ge-for-Si substituted synthetic clintonites (Cln), $CaMg_2(Al_{4-x}Ga_x)(Si_{1-y}Ge_y)O_{10}(OH,OD)_2$ (x = 0.0–4.0, y = 0.0–1.0). Rietveld analyses indicate that there is complete solid-solution in both the $(Al_{4-x}Ga_x)$Si-, $(Al_{4-x}Ga_x)$Ge-clintonite series. With increasing Ga-for-Al, the mean tetrahedral bond-length, <T-O>, and mean tetrahedral basal oxygen separation, $<^{[4]}O_{bas}\text{-}O_{bas}>$ increase, whereas the octahedral and interlayer parameters, the tetrahedral rotation angles (α), and the dimensional misfits (Δ) vary little. With increasing Ga-for-Al substitution in the Si-series the broad OH and OD stretching bands shift downward from 3607 to 3529 cm^{-1} and from 2671 to 2620 cm^{-1}, respectively. For the Ge-series samples, the OH and OD stretching bands shift downward from 3610 to 3523 cm^{-1} and from 2667 to 2611 cm^{-1}, respectively. According to the data of the curve fitting analysis, both the OH- and OD-stretching bands are modeled by at least three broad (wider than 37 cm^{-1} of full width at half height (FWHH)) I bands (M1M2M2 = $MgMgAl^{3+}$/$MgMgGa^{3+}$) and a narrow (FWHH = 23−33 cm^{-1}) and weak N band (M1M2M2 = MgMgMg) on the highest frequency side. In some samples, a very weak and broad V (one vacant M site) band at the lowest frequency region is observed.

Tetrahedral Si-O, Al-O and Ga-O stretching bands lie in fairly discrete regions, which are at 1030−830, 880−760 and 790−640 cm^{-1}, respectively. However, the band regions for both the tetrahedral Al-O and Ge-O stretching as well as the Ge-O and Ga-O stretching bands closely overlap each other. In the 720−500 cm^{-1} region, Si-O-Al, Al-O-Al, Si-O-Ga, Al-O-Ge, Al-O-Ga, Ge-O-Ga, and Ga-O-Ga deformational bands (tetrahedral-chain bending and "breathing" modes) are observed to overlap strongly. Around 300 and 200 cm^{-1} one observes the Ca-O_{inner} and Ca-O_{outer} stretching bands, respectively, which show a slight downward frequency shift (~ 7 cm^{-1} per Ga apfu) with Ga-for-Al substitution.

INTRODUCTION

Clintonite, a trioctahedral brittle mica with the ideal composition $Ca(Mg_2Al)(Al_3Si)O_{10}(OH,F)_2$, has several interesting characteristic crystal-chemical features (Takéuchi and Sadanaga 1959; Takéuchi 1966; Joswig et al. 1986; MacKinney et al. 1988; Alietti et al. 1997). First, its tetrahedral Al:Si ratio is 3:1, and thus half of the T-O-T bonds violate the Al-avoidance principle or the "Lowenstein avoidance rule" by having Al^{3+}-O-Al^{3+} bonds. Second, the tetrahedral cations are disordered and the tetrahedra are flattened as a consequence of the large Al content. Third, the large dimensional misfit of the tetrahedral and octahedral sheets is compensated by large tetrahedral rotation angles (α). Research on the synthesis and stability of clintonite has been done by Olesch (1975) and Olesch and Seifert (1976). Both mid- and far-infrared (MIR and FIR) spectra for synthetic and natural clintonites have been reported by Farmer and Velde (1973). Jenkins (1989), in addition to investigating MIR band assignments for synthetic phlogopites, also investigated synthetic clintonite and its deuterium (D), Ni-, Ga-, and Ge chemical analogues. The purpose of this paper is to further assign and characterize some MIR and FIR bands based on the X-ray Rietveld refinement data for synthetic $CaMg_2(Al_{4-x}Ga_x)SiO_{10}(OH)_2$- and $CaMg_2(Al_{4-x}Ga_x)GeO_{10}(OH)_2$-series clintonites, and their deuterated equivalents. In

addition, two synthetic Ni-bearing Si-clintonites, Ni_1SiH- and Ni_2SiH-Cln, were also examined; substitutions were made in the various sites in the clintonite structure in order to observe the influence of different ions on the spectra.

EXPERIMENTAL AND ANALYTICAL METHODS

The experimental and analytical methods in this study are similar to those of Ishida and Hawthorne (2011).

Synthesis

Experiments at 690–730 °C, 186–225 MPa and durations of 231–434 h were done in cold-seal Tuttle-type vessels. The starting materials were made from mixtures of reagent-grade oxides (MgO, NiO, Al_2O_3, Ga_2O_3, SiO_2, GeO_2) and carbonates ($CaCO_3$). The starting materials were mixed together and decarbonated by roasting for about 30 min. at approximately 900 °C in air, and then sealed in 5.0 mm outer-diameter × 4.7 mm inner-diameter × (~) 35 mm long Au capsules with ~20 wt% distilled water. Bulk compositions investigated in this study are given in Table 1. Deuteration experiments were done at about 600 ˚C, 200 MPa for a duration of 1 day in the same vessels; similar amounts of materials were used for the OD-bearing samples, using D_2O (99.9% purity)

with the solids sealed in Au capsules.

X-ray Rietveld analysis

Powder-diffraction data were collected with a Rigaku Rint-2100V diffractometer using Cu$K\alpha$ X-ray monochromatized with a curved-graphite and operating at 40 kV and 40 mA: more than 3000 counts were obtained for the strongest reflections with a step-width of 0.02 or 0.04° 2θ and count times of 4–10 s. Rietveld analysis was done using the program Rietan-2000 (Izumi and Ikeda 2000). The single crystal data for the Chichibu-mine clintonite from MacKinney et al. (1988) were used to initiate refinements. The clintonite structure was refined as the 1M polytype, with monoclinic space group *C2/m*, using isotropic displacement parameters, as the initial parameters for least-squares refinement. Three sets of data were averaged from Rietveld refinements done on three separate scans obtained with different X-ray conditions for a given sample.

Infrared spectroscopy

Both MIR and FIR spectra were recorded with a JASCO FTIR-620 spectrometer. The OH and OD stretching bands were recorded in the ranges of

4000–3000 and 3800–2000 cm^{-1} respectively. Samples were prepared as 150 mg KBr discs 10 mm in diameter and containing ~3 mg synthetic clintonite. Spectra were measured with 126 replicate scans at a nominal resolution of 1 cm^{-1}. After the background was substracted as a spline fit to the raw data, each spectrum was fitted to component pseudo-Voigt bands. The 1300–400 cm^{-1} bands were obtained from discs prepared with 100 mg KBr containing ~1 mg samples. Spectra were measured 64 times with a nominal resolution of 2 cm^{-1} in the 4000–400 cm^{-1} range. The 650–50 cm^{-1} and 250–30 cm^{-1} regions were recorded at a nominal resolution of 4 cm^{-1} with 10 mm diameter discs containing ~ 4 mg of sample in about 80 mg polyethelene discs. A globar light source with 5 μm Mylar beam splitter, and Hg-lamp with 12 μm Mylar beam splitter, respectively, were used with a PE-TGS detector.

RESULTS AND DISCUSSION

Products of synthesis

XRD indicated that ~ 90% of clintonite was obtained for each starting composition (Table 1), along with an amorphous phase of unknown composition (appearing as a hump in the diffraction pattern). Accordingly, compositional deviations are expected. As the $Ni_2SiHCln$ sample has large amounts of NiO (bunsenite), its FTIR

121 spectra were used only for comparisons. Chemical compositions for deuterated
122 materials may be similar to the OH-forms.
123
124 **X-ray Rietveld refinement**
125 All synthetic clintonites could be analyzed as the 1*M* polytype (Fig. 1). The
126 relatively large amounts of an amorphous phase were hard to model resulting in
127 agreement indices that are somewhat high; however, the resulting structural parameters
128 are considered to be sufficiently precise for the purposes of this study. Rietveld
129 refinement data, atom coordinates, and selected interatomic distances and angles are
130 given in Tables 2*, 3*, 4* and CIF *(deposit item #######). Definitions for the
131 structural parameters reported here are given in the footnotes of Table 4. The standard
132 deviations for the mean bond lengths involving T (= <T-O>), M (= <M1-O> and
133 <M2-O>) and I (= <I–O_{inner}>and <I–O_{outer} >) sites are estimated as ± 0.02, ± 0.04, and ±
134 0.05Å, respectively, though the individual bond distances and bond angles become
135 highly scattered. The standard deviations of the bond angles are estimated as ± 1˚.
136 **Cell dimensions.** The measured cell parameters of the synthetic clintonites are plotted
137 in Figure 2. Data points show smooth curved relations which support the presence of
138 continuous solid-solution series along the tetrahedral Al/Ga substitutions in each SiH-

and GeH-Cln series.

Site-populations. The tetrahedral and octahedral site populations obtained by the Rietveld analysis are plotted as a function of nominal Ga(apfu) of the starting materials in Figure 3. Compared with the 1:1 ideal population lines, the $^{[4]}$(Ga+Ge)/$^{[4]}$(Al+Si+Ga+Ge) values in the tetrahedral sites and $^{[6]}$Ga/$^{[6]}$(Mg+Al+Ga) values in the octahedral M1 and M2 sites are both lower than excepted, except for those of the end-member.

The T sites. The variation of the tetrahedral parameters as a function of $^{[4]}$(Ga +Ge)/$^{[4]}$(Al+Ga+Si+Ge) observed by Rietveld refinement are shown in Figure 4*. With increasing $^{[4]}$(Ga+Ge), the <T–O> bond lengths, the average separation of the basal oxygens of the tetrahedron (= <$^{[4]}O_{basal}$-O_{basal}>), and the thickness of the sheet of tetrahedra (t_t) all increase. The flattening angle of the tetrahedron ($\tau = \angle O_{apical}$-T-O_{basal}) also increases with increasing $^{[4]}$(Ga+Ge) content except for the end member Ga_4GeH-Cln. It is noted that the ideal flattening angle is 109.47˚ (Brigatti and Guggenheim 2002), and the flattening angle draws close to this value for the studied samples.

Octahedrally coordinated sites. The variations of the octahedral parameters observed by Rietveld refinement are not so large in both series (Fig. 5*), because only

157 one apfu $^{[6]}$Ga (r = 0.620 Å; Shannon 1976) for $^{[6]}$Al (r = 0.535 Å; ditto) is substituted
158 in both series.

159 **Interlayer sites.** The relations between the nominal Ga (apfu) and the interlayer-site
160 parameters are shown in Figure 6. In both SiH- and GeH-Cln series, the mean bond
161 lengths <I-O_{inner}> slightly decrease with increasing Ga, while the <I-O_{outer}> slightly
162 increase. Both basal oxygen angles, ∠O-O-O_{acute} and ∠O-O-O_{obtuse}, are nearly 60˚ and
163 180˚, respectively, and thus the tetrahedral basal oxygens make an isosceles triangle.
164 The interlayer separation (= interlayer sheet thickness) varies little.

165 **Rotation angles (α) and dimensional misfit** (Δ)**.** The tetrahedral rotation angles α
166 vary slightly between 27.8–29.6˚, and the dimensional misfit Δ increases in both series
167 (Fig. 7*). Except for Ga_3SiH- and Ga_4SiH-Cln, the angle α tends to increase slightly
168 with the dimensional misfit as well as with the mean separation of the tetrahedral basal
169 oxygens, <$^{[4]}O_{basal}$-O_{basal}> (Fig. 8*).

170

171 <Footnote>

172 * Deposit items. Tables 2, 3, 4, Figures 4, 5,7, 8, and CIF are deposited.

173 **IR spectra**

174 The clintonite IR spectra in both the MIR and FIR regions show the following

175 characteristic properties. (1) There are broad OH/OD stretching bands occurring in the
176 range of 3800–3000 cm^{-1} for OH strechings and in the range of 2800–2400 cm^{-1} for OD
177 stretchings. (2) The T-O stretching bands have widths ~ 100 cm^{-1} FWHH (full-width at
178 half -height) each and occur in separate Si-O, Al/Ge-O, Ge/Ga-O and Ga-O
179 vibrational-band regions. (3) There are combined strong T-O-T bending bands with
180 inarticulate O-T-O bendings occurring in the range of 750–550 cm^{-1}. (4) A couple of
181 medium bands appear in the 300–100 cm^{-1} FIR region.
182
183 **MIR spectra**
184 **OH and OD stretching bands (νOH and νOD modes).** There are broad OH and
185 OD stretching bands in both Si(H/D)- and Ge(H/D)-Cln series; their FWHH are more
186 than 100 cm^{-1} (Fig. 9). The OH stretching band of the synthetic Al_4SiH-Cln, labeled x =
187 0.0 in Figure 9a, is centered at 3607 cm^{-1} and is in very good agreement with the band
188 observed by Farmer and Velde (1973, labeled $S(SiAl_3)$). With increasing Ga content, the
189 band's center position shifts to lower frequencies in both the Si- and Ge-Cln series; the
190 frequencies of the OH/OD stretching bands in the Si-Cln series are slightly higher (~ 15
191 cm^{-1}) than those of the corresponding Ge-Cln series (Fig. 9). The observed OH and OD
192 stretching bands were analyzed into component bands (Table 5). In almost all samples,

193 the frequency ratios, νOH/νOD, for the corresponding bands lie in the range 1.36–1.33.
194 These shifts are very close to the calculated factor of 1.37 assuming a harmonic
195 oscillation (e.g., Jenkins 1989). The OH stretching bands I_D and I_E of which νOH/νOD
196 factors are ≈ 1.31 contain some adsorbed water. In most samples, a rather narrow and
197 weak shoulder band N (N = normal bands; Vedder 1964) on the high-frequency side of
198 the main bands appears; this N band is attributed to (MgMgMg)-OH/OD stretchings. Up
199 to five broad and strong bands I (I = impurity bands; Vedder 1964), I_A–I_E, are ascribed
200 to [MgMg(Al/Ga)]-OH/OD stretchings. In the deuterated samples SiD- and GeD-Clns,
201 a very weak and broad band V, where V is a vacancy (Vedder 1964), is observed at 2510
202 cm^{-1} and is ascribed to (MgMgV)-OH/OD stretchings.

203 **1300–400 cm^{-1} lattice vibration bands.** The bands in the 1300–400 cm^{-1} regions are
204 shown in Figure 10.

205 **(1) T-O stretching bands.** The regions of the tetrahedral Si-O and Al-O stretching
206 bands are well separated, as are the regions of the Si-O and Ga-O stretching bands, and
207 the band regions are completely different. For the Si-O and Ga-O stretching bands, there
208 are some shoulder bands at the low-frequency side. With increasing Ga→Al substitution
209 up to 1.0 Ga(apfu) in Si-Clns, the frequencies of the Si-O and Al-O stretching bands
210 decrease by 9 and 3 cm^{-1}, respectively, but the band intensity and shape do not change

211 so strongly. The intensities of the Ga-O stretching bands are rather low compared with
212 the Si-O and Al-O stretching bands (Fig. 10a).

213 **(2) T-O-T bending bands and weak O-T-O out-of-plane bands.** In the
214 $^{[4]}(T^{3+}_{3}T^{4+}_{1})$ tetrahedral sheet, there are the same number of T^{3+}-O-T^{3+} and T^{3+}-O-T^{4+}
215 linkages, while the T^{4+}-O-T^{4+} linkage will be very rare or nonexistent. In the 730–480
216 cm^{-1} range for the clintonites studied here, some bending and breathing bands ascribed
217 to these linkages should appear. With increasing Ga→Al substitution, two modes of a
218 broad and strong T-O-T bending band with a couple of shoulder bands are observed in
219 Figure 10.

220 Here, we examine the bands which appear in the 770–580 cm^{-1} range for the
221 tetrahedral $^{[4]}(Al_1Si_3)$, $^{[4]}(Al_2Si_2)$, and $^{[4]}(Al_3Si_1)$ micas. In the disordered tetrahedral
222 $^{[4]}(Al_1Si_3)$ trioctahedral mica such as phlogopite, 5 peaks of absorption bands are
223 observed in the 770–580 cm^{-1} range (Farmer 1974; Jenkins 1989): 760 cm^{-1} Si-O-Si
224 bending, 725 cm^{-1} Si-O-Al bending, 690 cm^{-1} O-Si-O out-of-plane bending, 655 cm^{-1}
225 O-Al-O out-of-plane bending, and 592 cm^{-1} OH librational band (δOH, in-plane OH
226 bending; Farmer 1974). The 690 cm^{-1} band intensity is roughly three times stronger than
227 that of the 655 cm^{-1} band, because there are three times more Si-O tetrahedra than Al-O
228 tetrahedra in phlogopite. In the ordered $^{[4]}(Al_2Si_2)$ trioctahedral mica such as margarite,

229 a diffuse but strong band at 681 cm^{-1} in synthetic 1*M* and 1*Md* polytypes was observed
230 (Velde 1980). This band in margarite is ascribed to the Si-O-Al bending, because there
231 is only the Si-O-Al tetrahedral linkage in the ordered $^{[4]}(Al_2Si_2)$ micas, which obey the
232 Al/Al avoidance rule. In the spectra for the synthetic 2*M* and natural margarite a
233 shoulder band at about 727 cm^{-1} was observed. Distinct O-T-O bending bands can not be
234 observed in the $^{[4]}(Al_2Si_2)$ micas.

235 Similar to the bands at 693 and 681 cm^{-1} in synthetic margarites by Farmer and
236 Velde (1973) and Velde (1980), the strong and broad bands at 661 and 667 cm^{-1} SiH-
237 and Ni_1SiH-Clns, respectively, are the bands for which the Si-O-Al and Al-O-Al
238 bending vibrations strongly overlap. These bands show a slightly positive skew shape
239 tailing to the lower frequency side and a weak shoulder band appears in Ga_4SiH- and
240 Ga_4GeH-Clns at 526 and 517 cm^{-1} (Fig. 10). They may probably be ascribed to the
241 O-$^{[4]}$Ga-O out-of-plane bending band. The sequence to lower frequencies of these T-O-T
242 bending bands depends primarily on the T-O bond lengths and then next on the mass of
243 T-site cations. Thus the T-O-T bands are assigned as the Si-O-Al, Al-O-Al, Si-O-Ga,
244 Al-O-Ga and Ga-O-Ga linkages in the Si-Cln series, and as the Al-O-Al, Al-O-Ge,
245 Al-O-Ga, Ge-O-Ga and Ga-O-Ga linkages in the Ge-Clns, respectively.

246 **(3) OD librational bands** (δOD mode)**.** Parts of the 617, 517, 546 and 512 cm^{-1}

247 weak bands in the deuterated clintonites, Al_4SiD-, Ga_4SiD-, Al_4GeD- and Ga_4GeD-Clns,
248 may be ascribed (partly) to OD librational bands (δOD = in-plane OD bending) as
249 demonstrated by the downward shift induced by deuteration, though their in-plane OH
250 bending bands (δOH) are obscure due to strong overlap with the Al/Ga-O stretching
251 bands.

252 **(4) M-O and T-O deformational bands.** Below 580 cm^{-1} in Si-Clns and 570 cm^{-1} in
253 Ge-Clns, several M-O and T-O deformational bands were observed, however, individual
254 band assignments are difficult because of strong overlaps.

255

256 **Low frequency vibrational bands including FIR bands**

257 Spectra in the 450–50 cm^{-1} low-frequency range, including the far infrared (FIR)
258 range below about 250 cm^{-1}, for synthetic clintonites are shown in Figures 11 and 12.

259 **(1) Absence of the tetrahedral torsional band in the FIR region.** Ishida and
260 Hawthone (2011) showed that the frequencies of the tetrahedral torsional vibrations in
261 synthetic kinoshitalites decrease linearly with increasing mean ionic radius of the
262 composite tetrahedra, $<^{[4]}r>$. Though the interlayer ion in clintonite is Ca^{2+} instead of
263 Ba^{2+} in kinoshitalite, the tetrahedral torsional band in the clintonites studied here should
264 appear below about 135 cm^{-1}, as the nominal tetrahedral ionic-radius range is

0.358–0.450 Å. However, no such bands are observed in Figures 11 and 12. On the other hand, Farmer and Velde (1973) reported very weak bands at 136–137 cm^{-1} in both natural and synthetic clintonites. This band frequency is in close accordance with the predicted values since $^{[4]}(Al_3Si_1)$ has $<^{[4]}r> = 0.358$ Å. Furthermore, they reported strong 145 cm^{-1} bands in natural and synthetic margarites; they are only attributed to the tetrahedral torsional bands when the mica tetrahedral composition is $^{[4]}(Al_2Si_2)$, i.e., $<^{[4]}r> = 0.325$ Å. It is unclear why the tetrahedral torsional band does not appear in the synthetic clintonites studied here.

(2) $Ca\text{-}O_{inner}$ and $Ca\text{-}O_{outer}$ stretching bands. Two medium-strong bands centered at 300–279 (290 av.) and 195–181 (188 av.) cm^{-1} for the Si-Cln series, and at 304–283 (294 av.) and 196–181 (188 av.) cm^{-1} for the Ge-Cln series were observed. Farmer and Velde (1973) reported these bands without assignment. Jenkins (1989) also observed a weak 300 cm^{-1} band in synthetic clintonites. In Figure 13, the frequencies of the FIR bands for synthetic $^{[4]}(Al_1Si_3)$ and $^{[4]}(Al_2Si_2)$ trioctahedral micas (phlogopite and kinoshitalite, respectively) with various interlayer cations were plotted against $\sqrt{}$ (Z/M), where Z is the cation valency and M its molecular mass (cf. Fripiat 1982). Except for the lower frequencies of K-phlogopite, both lines exhibit quadratic curvature and the differences between the high- and low-frequency bands increase with increasing $\sqrt{}$

283 (Z/M). Fripiat (1982) assigned these high-frequency bands as out-of-plane vibrational
284 bands of interlayer cations and the low-frequency bands as in-plane vibrational bands of
285 the interlayer cations, respectively. However, these assignments can hardly explain the
286 relationships between the crystal-chemical parameters and the band frequencies. For
287 example, the F-bearing kinoshitalites have shorter *c*-parameters than OH-bearing ones,
288 and thus should give higher-frequency out-of-plane vibrations of the interlayer cation,
289 but in reality, the band frequencies shift downward with increasing F→OH/OD (Ishida
290 and Hawthorne 2011). Figure 14 shows the variation in <I-O> bond length (I = Ca) as a
291 function of Ga (apfu). The nearly 100 cm^{-1} frequency differences between these two
292 medium-strong bands should be ascribed to Ca-O_{inner} and Ca-O_{outer} stretching bands
293 corresponding to their large <I-O_{outer}> and <I-O_{inner}> differences. In natural margarite
294 two bands at 280 and 180 cm^{-1}, which were reported by Farmer and Velde (1973), may
295 be Ca-O_{inner} and Ca-O_{outer} stretching bands, respectively. However, frequencies of these
296 bands are lower than those of clintonites by ~ 10 cm^{-1} due to crystal-chemical
297 differences, such as the tetrahedral Al:Si = 1:1 and dioctahedral characteristics of the
298 natural margarite.

299 **(3) M-O and OH librational (γOH mode) bands.** Two weak bands centered at
300 267–231 and 215–214 cm^{-1} were observed in Al-rich samples of both series (Fig. 11).

With increasing Ga content the intensity of both bands decreases. The frequency for the former bands decrease in samples with more than 2.0 Ga, however, the frequency for the latter bands does not shift. These bands are therefore assigned to M-O librational (rocking) modes. A weak band around 400 cm^{-1} in SiH- and GeH-Clns may be partly ascribed to out-of-plane OH bending (γOH), because the intensity decreases slightly by deuteration (Fig. 11a).

ACKNOWLEDGMENTS

The author thanks D.M. Jenkins for his valuable discussions and constructive comments. H. Kojitani gave advices that was usuful in making CIFs. The author is indebted to A. Beran, H. Skogby and S. Stalder for their critical reading of the manuscript, helpful suggestions and many recommendations. Infrared spectra were recorded at the Center of Advanced Instrumental Analysis, Kyushu University. K.I. was supported by a Subsidy of an excellent study of the Graduate School of Social and Cultural Studies, Kyushu University, and partly supported by a Grand-in-Aid for Scientific Research for Y. Kuwahara (No. 23340163).

REFERENCES CITED

Alietti, E., Brigatti, M.F., and Poppi L. (1997) Clintonite-1*M*: Crystal chemistry and its relationships to closely associated Al-rich phlogopite. American Mineralogist, 82, 936–945.

Brigatti, M.F. and Guggenheim, S. (2002) Mica crystal chemistry and the influence of pressure, temperature, and solid solution on atomistic models. In *Micas:Crystal Chemistry & Metamorphic Petrology*, 351–369 (A. Mottana, F.P. Sassi, J.B. Thompson,Jr., and Guggenheim, editors). Reviews inMineralogy & Geochemistry, 46, Mineralogical Society of America and the Geochemical Society, Washington, DC.

Donnay, G., Donnay, J.D.H., and Takeda, H (1964) Trioctahedral one-layer micas. Prediction of the structure from composition and cell dimensions. Acta Crystallographica, 17, 1374–1381.

Farmer, V.C. (1974) Layer silicates. In: *Infrared spectra of minerals*. Ed. V.C. Farmer, Mineralogical Society London, 331–360.

Farmer, V.C. and Velde, B. (1973) Effects of structural order and disorder on the infrared spectra of brittle micas. Mineralogical Magazine, 39, 282–288.

Fripiat, J.J. (1982) Application of far infrared spectroscopy of the study of clay minerals and zeolites. In: *Developments in sedimentology*, 34, J.J.Fripiat (ed). Advancedtechniques for clay mineral analysis, 191–210, Elsevier Scientific Pub. Co.

Hazen, R.M. and Burnham, C.W. (1973) The crystal structures of one-layer phlogopite and annite. American Mineralogist, 58, 889–900.

Ishida, K. and Hawthorne, F. (2011) Far-infrared spectra of synthetic $^{[4]}[(Al_{2-x}Ga_x)(Si_{2-y}Ge_y)](OH,OD,F)_2$-kinoshitalite: Characterization and assignment of interlayer Ba-O_{inner} and Ba-O_{outer} stretching bands. American Mineralogist, 96, 566–576.

Izumi, F. and Ikeda, T. (2000) A Rietveld analysis program RIETAN -98 and its application to zeolites. Material Science Forum, 321–324.

Jenkins, D.M. (1989) Empirical study of the infrared lattice vibrations (1100–350 cm^{-1}) of phlogopite. Physics and Chemistry of Minerals, 16, 408–414.

Joswig, W., Amthaner, G., and Takeuchi, Y. (1986) Neutron diffraction and Mössbauer spectroscopic study of clintonite (xanthophyllite). American Mineralogist, 71, 1194–1197.

McKinney, J.A., Mora, C.I., and Bailey, S.W. (1988) Structure and crystal chemistry of clintonite. American Mineralogist, 73, 365–375.

Olesch, M. (1975) Synthesis and solid solubility of trioctahedral brittle micas in the system CaO-MgO-Al_2O_3-SiO_2-H_2O. American Mineralogist, 60, 188–199.

Olesch, M. and Seifert, F. (1976) Stability and phase relations of trioctahedral calcium brittle micas (clintonite group). Journal of Petrology, 17, 291–314.

Shannon, R.D. (1976) Revised effective ionic radii and systematic atudies of interatomic distances in halides and chalcogenides. Acta Crystallographica, A32, 751–767.

Takéuchi, Y. (1966) Structural studies of brittle micas (I). The structure of xanthophyllite refined. Mineralogical Journal (Japan), 4, 424–437.

Takéuchi, Y. and Sadanaga, R. (1959) The crystal structure of xanthophyllite. Acta Crystalloggraphica, 12, 945–946.

Toraya, H. (1981) Distortions of octahedra and octahedral sheets in 1*M* micas and the relation to their stability. Zeitschrift für Kristallography, 157, 173–190.

Vedder, W. (1964) Correlations between infrared spectrum and chemical composition of mica. American Mineralogist, 49, 736–768.

Velde, B. (1980) Cell dimensions, polymorph type, and infrared spectra of synthetic white micas: the importance of ordering. American Mineralogist, 65, 1277–1282.

Captions of figures.

FIGURE 1. Rietveld patterns of synthetic clintonite. (**a**) [876]SiHCln. (**b**) [916]Ga_4GeHCln. The crosses are the observed data, the solid line is the calculated pattern, and the vertical bars mark all possible Bragg reflections (Cu$K\alpha_1$ and Cu$K\alpha_2$). The difference between the observed and calculated patterns is shown at the bottom.

FIGURE 2. Cell parameters and site populations of synthetic clintonite fitted to a quadratic function by least-squares regression. Open circles: $(Al_{4-x}Ga_x)$SiH-Cln series. Solid circles: $(Al_{4-x}Ga_x)$GeH-Cln series. Open square: $Si_{0.5}Ge_{0.5}$HCln. Solid triangle: Ni_1SiHCln. Open diamond: Ni_2SiHCln. Solid and broken lines: least-squares regression lines for Si- and Ge-Cln series, respectively. Errors for unit-cell dimensions and volumes are smaller than the dimensions of the symbols.

FIGURE 3. **(a)** Ga+Ge site-populations in the tetrahedral sites, and (**b**) Ga site-populations in the octahedral M1 and M2 sites, estimated by X-ray Rietveld refinements. Open circles: $(Al_{4-x}Ga_x)$SiH-Cln series. Solid circles: $(Al_{4-x}Ga_x)$GeH-Cln series. Open square: $Si_{0.5}Ge_{0.5}$H-Cln. Samll circles: M1 sites. Large circles : M2 sites. Solid lines: theoretical 1:1 correlation lines. Broken

389 lines: quadratic function least-squares regression lines of observed site-populations.

390

391 (*: Deposit items)

392 ***FIGURE 4.** Variation in tetrahedron parameters as a function of the nominal Ga

393 (apfu) for the starting material fitted to a quadratic function by least-squares

394 regression lines. Both the Si- and Ge-Cln data are modeled with the same curve.

395 (**a**) <T-O> = mean tetrahedral bond-length. (**b**) τ = tetrahedral flattening angle.

396 (**c**) $<^{[4]}O_{basal}\text{-}O_{basal}>$ = mean separation of basal oxygens of the tetrahedron. (**d**) t_t =

397 tetrahedral sheet thickness. Solid triangles: Ni_1SiH- & Ni_2SiH-Clns. Other

398 legends as in Fig. 2. Definitions for the structural parameters see note in Table 4.

399

400 ***FIGURE 5.** Variation in octahedron parameters as a function of the nominal Ga (apfu)

401 for the starting material fitted to a quadratic function by least-square regression

402 lines. Both the Si- and Ge-Cln data are modeled with the same curve. (**a**) <M1,2

403 -O> = mean octrahedron bond-length. (**b**) $\Psi_{M1,M2}$ = octahedron flattening angle.

404 (**c**) t_o = tetrahedral sheet thickness. Legend as in Fig. 4.

405

406 **FIGURE 6.** Variation in interlayer-site parameters as a function of the nominal Ga

(apfu) for the starting material fitted to a quadratic function by least-squares regression. (**a**) <I-O_{inner}> = mean inner interlayer bond-length, <I-O_{outer}> = mean outer interlayer bond-length. (**b**) ∠O-O-O_{acute} = mean acute interlayer oxygen angle, ∠O-O-O_{obtuse} = mean obtuse interlayer oxygen angle. (**c**) t_i = interlayer sheet thickness. Legend as in Fig. 4.

FIGURE 7. Variation in (**a**) α = the rotation angles of the tetrahedron, and (**b**) Δ = the dimensional misfit, both as a function of the nominal Ga (apfu) for the starting material fitted to a quadratic function by least-squares regression. Legend as in Fig. 4.

FIGURE 8. Variations in α as functions of (**a**) the mean separation of basal oxygens of the tetrahedron (= <$^{[4]}O_{basal}$-O_{basal}>) and (**b**) the dimensional misfit (Δ) shown by quadratic-function least-squares regression curves.

FIGURE 9. Infrared OH and OD stretching bands of synthetic clintonite. **(a)** $(Al_{4-x}Ga_x)$SiH-Cln series; x= 0.0–2.0. **(b)** $(Al_{4-x}Ga_x)$SiH-Cln series; x= 3.0–4.0. $Si_{0.5}Ge_{0.5}$H-, Ni_1SiH-, and Ni_2SiH-Clns . (**c**) $(Al_{4-x}Ga_x)$GeH-Cln series. **(d)**

425 $(Al_{4-x}Ga_x)$SiD-Clns; x = 0.0, 2.0 and 4.0. $(Al_{4-x}Ga_x)$GeD-Clns; x = 0.0, 2.0 and 4.0.

426 Solid lines: observed spectra and individual components analyzed. Broken lines:

427 sum of the analyzed components. Lines have been displaced vertically for clarity.

428 N = normal, I_A–I_E = impurity, and V = vacant bands (Vedder 1964).

429

430 **FIGURE 10.** Infrared spectra (1300–400 cm^{-1}) of synthetic clintonite. **(a)**

431 $(Al_{4-x}Ga_x)$Si-Cln series. (**b**) $(Al_{4-x}Ga_x)$Ge-Cln series, $Si_{0.5}Ge_{0.5}$H-, Ni_1SiH-, and

432 Ni_2SiH-Clns. Solid lines = OH-forms. Broken lines = OD-forms.

433

434 **FIGURE 11.** Far -infrared spectra (450–100 cm^{-1}) of synthetic clintonite. (**a**)

435 $(Al_{4-x}Ga_x)$Si-Cln series. $Si_{0.5}Ge_{0.5}$H-, Ni_1SiH-, and Ni_2SiH-Clns. (**b**)

436 $(Al_{4-x}Ga_x)$Ge-Cln series. Solid lines = OH-forms. Broken lines = OD-forms.

437

438 **FIGURE 12.** Far -infrared spectra (250–50 cm^{-1}) of synthetic clintonite. (**a**)

439 $(Al_{4-x}Ga_x)$Si-Cln series. $Si_{0.5}Ge_{0.5}$H-, Ni_1SiH-, and Ni_2SiH-Clns. (**b**)

440 $(Al_{4-x}Ga_x)$Ge-Cln series. Solid lines = OH-forms. Broken lines = OD-forms.

441

442 **FIGURE 13.** Interlayer cation frequencies observed for synthetic micas vs. $\sqrt{(Z/M)}$

443 modeled with quadratic-function least-squares regression curves. Z = valence of the
444 interlayer cation. M = atomic mass of the interlayer cation. Ca^{2+}: clintonite (this
445 study, [875]). $K^{+}/Rb^{+}/Cs^{+}$: phlogopites (Ishida, unpublished data). Sr^{2+}:
446 Fluoro-Sr-kinoshitalite (Ishida, unpublished data). Ba^{2+}: kinoshitalites (Ishida and
447 Hawthorne 2011, samples [811]Al_2Si_2Kn and [M30]$F2Al_2Si_2Kn$). Circles:
448 (OH)-bearing micas. Triangles: F-bearing micas.
449
450 **FIGURE 14.** Variation in <I-O> bond-lengths as a function of the nominal Ga (apfu)
451 for the starting material modeled by quadratic least-squares regression curves. (**a**)
452 $(Al_{4-x}Ga_x)$SiH-Cln series (open circles and solid squares), $Si_{0.5}Ge_{0.5}$H-Cln
453 (triangles) and Ni_1SiH-Cln (diamonds). (**b**) $(Al_{4-x}Ga_x)$GeH-Cln series. Solid and
454 broken lines: least-square regression lines for the components of <I-O_{outer}> and
455 -O_{inner}>, respectively (see text).
456
457

TABLE 1. Hydrothermally synthesized clintonites and MIR & FIR band's assignments

Run no.	Symbol	Nominal composition	*T* (C)	*P* (MPa)	*t* (h)	OH str.
		(a) $(Al_{4-x}Ga_x)$Si-Cln series				
[875]	SiHCln	$Ca(Mg_2Al_1)(Al_3Si_1)O_{10}(OH)_2$	690	186	373	3742,3687,3618,3558,3423
[894]	$Ga_{0.5}$SiHCln	$Ca(Mg_2Al_1)(Al_{2.5}Ga_{0.5}Si_1)O_{10}(OH)_2$	710	196	374	3739,3676,3606,3538,3414
[876]	Ga_1SiHCln	$Ca(Mg_2Al_1)(Al_2Ga_1Si_1)O_{10}(OH)_2$	690	186	373	3733,3657,3588,3519,3418
[895]	$Ga_{1.5}$SiHCln	$Ca(Mg_2Al_1)(Al_{1.5}Ga_{1.5}Si_1)O_{10}(OH)_2$	710	196	374	3725,3649,3579,3505,3412
[877]	Ga_2SiHCln	$Ca(Mg_2Al_1)(Al_1Ga_2Si_1)O_{10}(OH)_2$	690	186	373	3725,3656,3590,3532,3436
[878]	Ga_3SiHCln	$Ca(Mg_2Al_{0.5}Ga_{0.5})(Al_{0.5}Ga_{2.5}Si_1)O_{10}(OH)_2$	690	186	373	3716,3652,3590,3530,3454,3374
[879]	Ga_4SiHCln	$Ca(Mg_2Ga_1)(Ga_3Si_1)O_{10}(OH)_2$	690	186	373	3709,3644,3592,3529,3446,3370
[885]	$Si_{0.5}Ge_{0.5}$HCln	$Ca(Mg_2Al_1)(Al_3Si_{0.5}Ge_{0.5})O_{10}(OH)_2$	710	225	231	3687,3619,3565,3444
[887]	Ni_1SiHCln	$Ca(Mg_1Ni_1Al_1)(Al_3Si_1)O_{10}(OH)_2$	710	225	231	3632,3578,3520,3410
[888]	Ni_2SiHCln	$Ca(Ni_2Al_1)(Al_3Si_1)O_{10}(OH)_2$	710	225	231	3632,3605,3548,3490,3415
		(b) $(Al_{4-x}Ga_x)$Ge-Cln series				
[886]	GeHCln	$Ca(Mg_2Al_1)(Al_3Ge_1)O_{10}(OH)_2$	710	225	231	3690,3618,3571,3437
[902]	Ga_1GeHCln	$Ca(Mg_2Al_1)(Al_2Ga_1Ge_1)O_{10}(OH)_2$	730	201	357	3677,3613,3573,3520,3418
[903]	Ga_2GeHCln	$Ca(Mg_2Al_1)(Al_1Ga_2Ge_1)O_{10}(OH)_2$	730	201	357	3664,3593,3555,3488,3388
[915]	Ga_3GeHCln	$Ca(Mg_2Al_1)(Ga_3Ge_1)O_{10}(OH)_2$	715	210	434	3649,3584,3543,3470,3385
[916]	Ga_4GeHCln	$Ca(Mg_2Ga_1)(Ga_3Ge_1)O_{10}(OH)_2$	715	210	434	3624,3524,3455,3387,3563

* Frequency difference between Ca-O_{inner} and Ca-O_{outer} stretching bands.

† : Numbers in parentheses are those for deuterated form.

OD str.	T-O str.	T-O-T bend.	O-T-O def.	M-O def.	M-O def. &T-O def.	Ca-O_{inner} str.	M-O def	M-O def.
(2757,2725,2692,2660,2620,2511)†	940,904,813	661	(617)	562(557)	505,488,451	300	261	214
	937,900,811	657,596		560	482,453,403	300,290	262,255	213
	931,896,810,722	650,594		556	474,452,411	294	258	213
	928,894,804,637	637,595,555			468,445,412	289	256	215
(2746,2709,2674,2638,2601)	925,893,794,778	640,589			455,445,414	292	255	
	918,890,754,687	584			446,436,417	286	250	
(2737,2689,2652,2620,2593,2552)	911,880,736,711,685	600,580	526(517)		442,429,415	279		
	947,810	652,598		557	481,454	300	263	214
	931,900,818	667		551	506,491,463,443,431	293	264,257	
	969,924,859,841	670,618		543	488,462,445,431,413	299	267,243	
(2719,2679,2660,2626,2508)	852,800,737,701	635,603		549(546)	493,469,439,357	304	263	215
	840,790,750	534,607			659,431,360	290	263	215
(2702,2661,2635,2594,2520)	818,770,686	597,554			459,444,432,418	284	251	
	832,789,744,676	618,580,559			443,429,415	283		
(2679,2633,2606,2558)	876,835,774,726,683	586,564,517	(512)		427,418	283	248,231	

Ca-O_{outer} str.	
195	105
193,189	104
192	102
191	98
189	103
185	101
181	98
196	104
199	94
200,186	99
196	108
194	96
190	94
186	97
181	102

TABLE 2. Rietveld refinement of (Al/Ga)(Si/Ge)(OH)-clintonite

Run no.	875	894	876	895	877	878	879	885	887	888	886	902	903	915	916
Symbol	SiHCln	$Ga_{0.5}$SiHCln	Ga_1SiHCln	$Ga_{1.5}$SiHCln	Ga_2SiHCln	Ga_3SiHCln	Ga_4SiHCln	$Si_{0.5}Ge_{0.5}$HCln	Ni_1SiHCln	Ni_2SiHCln	GeHCln	Ga_1GeHCln	Ga_2GeHCln	Ga_3GeHCln	Ga_4GeHCln
***T*(C)–*P*(MPa)**	690–186	710-196	690-186	710-196	690-186	690-186	690-186	710-225	710-225	710-225	710-225	730-201	730-201	715-210	715-210
Collecting conditions															
2 scan range (°)	5-120	5-120	5-120	5-120	5-120	5-120	5-110	5-120	5-120	5-120	5-120	5-120	5-120	5-120	5-120
Step interval (°)	0.04	0.02	0.02	0.04	0.04	0.04	0.01	0.04	0.04	0.04	0.04	0.02	0.04	0.04	0.04
Step times (s)	2	5	7	6	7	6	7	6	5	6	6	6	6	6	6
Agreement indicies from Rietveld refinement															
*R*wp(%)	26.2	25.7	26.7	25.7	28.7	26.9	32.1	25.9	22.2	29.4	32.5	30.5	19.8	23.3	29.8
*R*p(%)	20.7	20.6	21.1	20.1	22.8	21.2	28.1	20.7	17.0	22.2	24.7	25.6	15.2	18.3	23.9
*R*e(%)	7.89	5.50	5.78	4.19	6.10	3.96	5.46	4.22	5.00	4.56	4.40	4.49	4.00	3.95	3.95
S	3.32	4.67	4.61	6.14	4.70	6.81	5.87	6.13	4.44	6.43	7.39	6.79	4.96	5.90	7.56
Durbin-Watson *d*	0.122	0.048	0.054	0.089	0.146	0.125	0.015	0.118	0.117	0.376	0.072	0.041	0.177	0.141	0.127
R_F(%)	9.59	7.89	11.0	8.62	11.7	8.61	16.6	11.0	7.69	17.9	13.8	17.5	6.09	7.94	11.0
Unit-cell parameters															
a( )	5.2017(13)	5.2092(13)	5.221(2)	5.2314(16)	5.2427(13)	5.2704(15)	5.2983(13)	5.2198(18)	5.1902(13)	5.160(2)	5.2346(18)	5.2584(11)	5.2759(9)	5.3031(9)	5.3268(11)
b( )	8.991(2)	9.008(2)	9.025(3)	9.052(3)	9.068(2)	9.111(2)	9.161(2)	9.028(3)	8.975(2)	8.969(4)	9.056(3)	9.0973(19)	9.1352(15)	9.1773(16)	9.216(2)
c( )	9.799(2)	9.818(2)	9.841(4)	9.866(3)	9.882(2)	9.924(3)	9.960(2)	9.840(23)	9.806(2)	9.802(4)	9.870(3)	9.918(2)	9.9541(14)	9.9954(16)	10.023(2)
□(°)	100.142(16)	100.221(14)	100.120(17)	100.132(17)	100.085(15)	100.018(16)	100.034(12)	100.157(17)	100.187(16)	100.24(2)	100.35(2)	100.221(11)	100.260(9)	100.216(11)	100.172(15)
V(^{3})	451.13(19)	453.39(19)	456.5(3)	459.9(2)	462.5(2)	469.22(2)	476.0(2)	456.4(3)	449.58(18)	446.4(3)	460.3(3)	466.22(17)	472.08(13)	478.75(14)	484.31(18)
asin □( )	5.121(1)	5.126(1)	5.140(2)	5.150(2)	5.162(1)	5.191(1)	5.217(2)	5.138(2)	5.108(1)	5.078(2)	5.149(1)	5.175(4)	5.191(1)	5.219(2)	5.243(3)
*D*cal(g/cm^3)	3.123(5)	2.879(120)	2.950(110)	2.943(107)	3.095(43)	3.499(16)	3.657(209)	2.985(40)	3.116(27)	3.036(29)	3.318(135)	3.003(238)	3.383(15)	3.524(51)	4.556(21)
Site-populations															
T1 Ge+Ga	-	0.10(1)	0.11(1)	0.14(1)	0.19(2)	0.41(2)	0.70(4)	0.06(1)	-	-	0.21(3)	0.40(1)	0.47(1)	0.61(1)	1.00
Si+Al	1.00	0.90(1)	0.89(1)	0.86(1)	0.81(2)	0.59(2)	0.30(4)	0.94(1)	1.00	1.00	0.79(3)	0.60(1)	0.53(1)	0.39(1)	-
M1 Ga	-	0.00(1)	0.00(1)	0.00(1)	0.04(2)	0.17(3)	0.39(4)	-	Ni:0.24(2)	Ni:0.44(3)	-	0.02(1)	0.01(1)	0.12(1)	0.42(4)
Mg+Al	1.00	1.00(1)	1.00(1)	1.00(1)	0.96(2)	0.83(3)	0.61(4)	1.00	Al:0.76(2)	Al:0.56(3)	1.00	0.98(1)	0.99(1)	0.88(1)	0.58(4)
M2 Ga	-	0.00(1)	0.00(1)	0.00(1)	0.01(1)	0.20(2)	0.42(4)	-	Ni:0.19(1)	Ni:0.23(2)	-	0.00(1)	0.00(1)	0.08(1)	0.40(3)
Mg+Al	1.00	1.00(1)	1.00(1)	1.00(1)	0.99(1)	0.80(2)	0.58(4)	1.00	Al:0.81(1)	Al:0.77(2)	1.00	1.00(1)	1.00(1)	0.92(1)	0.60(3)
Average(M1+2M2)															
Ga	-	0.00(1)	0.00(1)	0.00(1)	0.02(1)	0.19(1)	0.41(1)	-	Ni:0.21(2)	Ni:0.30(10)	-	0.01(1)	0.01(1)	0.09(2)	0.41(1)
Mg+Al	1.00	1.00(1)	1.00(1)	1.00(1)	0.98(1)	0.81(1)	0.59(1)	1.00	Al:0.79(2)	Al:0.70(10)	1.00	0.99(1)	0.99(1)	0.91(2)	0.59(1)
A Ca	0.74(1)	0.77(1)	0.65(1)	0.60(2)	0.54(2)	0.68(2)	0.76(3)	0.73(2)	0.78(1)	0.67(2)	0.76(3)	0.73(1)	0.72(1)	0.63(2)	0.78(3)

TABLE 3. Atomic parameters of (Al/Ga)(Si/Ge)(OH/OD)-clintonite

Run no.		875	894	876	895	877	878	879	885	887	888	886	902	903	915	916
Symbol		SiHCln	$Ga_{0.5}$SiHCln	Ga_1SiHCln	$Ga_{1.5}$SiHCln	Ga_2SiHCln	Ga_3SiHCln	Ga_4SiHCln	$Si_{0.5}Ge_{0.5}$HClr	Ni_1SiHCln	Ni_2SiHCln	GeHCln	Ga_1GeHCln	Ga_2GeHCln	Ga_3GeHCln	Ga_4GeHCln
T-P		690–186	710-196	690-186	710-196	690-186	690-186	690-186	710-225	710-225	710-225	710-225	730-201	730-201	715-210	715-210
	x	0.550(2)	0.5573(15)	0.5527(17)	0.556(2)	0.553(2)	0.5523(18)	0.5584(13)	0.552(2)	0.558(2)	0.532(3)	0.584(3)	0.5604(18)	0.5662(15)	0.5627(14)	0.558(2)
T1	y	0.1697(11)	0.1668(8)	0.1699(8)	0.1681(9)	0.1685(9)	0.1692(8)	0.1689(6)	0.1683(9)	0.1706(8)	0.1650(17)	0.1664(12)	0.1680(8)	0.1665(5)	0.1669(5)	0.1668(7)
	z	0.2067(8)	0.2053(5)	0.2028(6)	0.2033(7)	0.2033(8)	0.2017(7)	0.2032(5)	0.2049(7)	0.2057(7)	0.1957(13)	0.2102(9)	0.2078(6)	0.2074(3)	0.2071(4)	0.2059(6)
	x	0	0	0	0	0	0	0	0	0	0	0	0	0	0	0
M1	y	1/2	1/2	1/2	1/2	1/2	1/2	1/2	1/2	1/2	1/2	1/2	1/2	1/2	1/2	1/2
	z	1/2	1/2	1/2	1/2	1/2	1/2	1/2	1/2	1/2	1/2	1/2	1/2	1/2	1/2	1/2
	x	1/2	1/2	1/2	1/2	1/2	1/2	1/2	1/2	1/2	1/2	1/2	1/2	1/2	1/2	1/2
M2	y	0.3308(13)	0.3291(13)	0.3231(13)	0.3239(17)	0.3265(18)	0.3286(16)	0.3248(12)	0.3297(15)	0.3300(10)	0.3285(16)	0.329(3)	0.3239(19)	0.3278(12)	0.3261(14)	0.3251(19)
	z	1/2	1/2	1/2	1/2	1/2	1/2	1/2	1/2	1/2	1/2	1/2	1/2	1/2	1/2	1/2
	x	1/2	1/2	1/2	1/2	1/2	1/2	1/2	1/2	1/2	1/2	1/2	1/2	1/2	1/2	1/2
A	y	1/2	1/2	1/2	1/2	1/2	1/2	1/2	1/2	1/2	1/2	1/2	1/2	1/2	1/2	1/2
	z	0	0	0	0	0	0	0	0	0	0	0	0	0	0	0
	x	0.088*	0.088*	0.088*	0.088*	0.088*	0.088*	0.088*	0.088*	0.088*	0.088*	0.088*	0.088*	0.088*	0.088*	0.088*
H	y	0	0	0	0	0	0	0	0	0	0	0	0	0	0	0
	z	0.303*	0.303*	0.303*	0.303*	0.303*	0.303*	0.303*	0.303*	0.303*	0.303*	0.303*	0.303*	0.303*	0.303*	0.303*
	x	0.389(7)	0.386(3)	0.414(5)	0.415(7)	0.378(7)	0.390(8)	0.423(5)	0.374(7)	0.378(6)	0.348(8)	0.394(14)	0.433(4)	0.375(4)	0.429(5)	0.396(14)
O1	y	0	0	0	0	0	0	0	0	0	0	0	0	0	0	0
	z	0.158(2)	0.1536(15)	0.145(2)	0.141(3)	0.148(3)	0.150(3)	0.152(2)	0.151(2)	0.1511(19)	0.147(3)	0.157(4)	0.1515(19)	0.1517(18)	0.149(2)	0.154(5)
	x	0.845(5)	0.864(2)	0.896(5)	0.905(5)	0.863(6)	0.846(6)	0.885(5)	0.855(5)	0.841(4)	0.832(6)	0.866(12)	0.897(4)	0.861(3)	0.911(4)	0.872(14)
O2	y	0.1598(18)	0.1619(13)	0.1571(13)	0.1598(18)	0.1592(19)	0.157(2)	0.1522(17)	0.1659(19)	0.1621(15)	0.148(2)	0.169(3)	0.1677(18)	0.1701(16)	0.1638(19)	0.160(4)
	z	0.1436(13)	0.1395(9)	0.1392(13)	0.1358(18)	0.1347(19)	0.127(2)	0.1324(13)	0.1441(14)	0.1414(11)	0.1315(15)	0.142(2)	0.1412(11)	0.1398(11)	0.1395(13)	0.143(3)
	x	0.625(4)	0.630(2)	0.599(3)	0.597(5)	0.605(5)	0.595(5)	0.598(4)	0.609(6)	0.634(5)	0.629(6)	0.643(9)	0.609(3)	0.637(4)	0.602(4)	0.632(9)
O3	y	0.168(2)	0.1687(14)	0.1685(17)	0.169(2)	0.170(2)	0.172(3)	0.171(2)	0.171(2)	0.1691(18)	0.163(2)	0.172(4)	0.1720(17)	0.1717(16)	0.1722(19)	0.170(4)
	z	0.3925(15)	0.3951(10)	0.3960(15)	0.3993(18)	0.400(2)	0.404(2)	0.3912(15)	0.3912(15)	0.3876(12)	0.3769(18)	0.403(3)	0.3981(12)	0.3981(10)	0.4007(13)	0.404(3)
	x	0.648(8)	0.653(4)	0.603(5)	0.603(7)	0.621(7)	0.621(8)	0.600(5)	0.629(6)	0.662(7)	0.612(7)	0.653(14)	0.592(4)	0.639(4)	0.589(4)	0.626(13)
O4	y	1/2	1/2	1/2	1/2	1/2	1/2	1/2	1/2	1/2	1/2	1/2	1/2	1/2	1/2	1/2
	z	0.400(2)	0.4056(14)	0.4026(18)	0.404(3)	0.404(3)	0.411(3)	0.3983(20)	0.401(2)	0.4001(17)	0.374(3)	0.401(4)	0.3930(18)	0.3984(16)	0.3924(19)	0.392(4)

Note : Following isotropic temperature facrors (B) were used: T = 1.06, M1 = 0.95, M2 = 1.08, A = 1.69, H = 1.70, O1 =2.70, O2 = 2.00,O3 = 1.12, O4 =1.80.

*: Fixed values.

TABLE 4. Crystal structure data of (Al/Ga)(Si/Ge)(H/D)-clintonite

Run no.		**875**	**894**	**876**	**895**	**877**	**878**	**879**
Symbol		SiHCln	$Ga_{0.5}$SiHCln	Ga_1SiHCln	$Ga_{1.5}$SiHCln	Ga_2SiHCln	Ga_3SiHCln	Ga_4SiHCln
T **(C)–*P*** **(MPa)**		690–186	710–196	690–186	710–196	690–186	690–186	690–186
Selected bond-lengths (Å)								
T-O1		1.766(16)	1.784(8)	1.749(11)	1.765(20)	1.826(19)	1.797(20)	1.745(10)
T-O2		1.753(27)	1.827(14)	2.005(26)	2.050(28)	1.875(31)	1.829(29)	1.982(23)
T-O2'		1.908(20)	1.904(10)	1.825(14)	1.830(19)	1.925(20)	1.993(22)	1.952(17)
T-O3		1.794(13)	1.845(9)	1.877(13)	1.910(17)	1.917(19)	1.985(21)	1.848(14)
<T-O>		1.805	1.840	1.864	1.889	1.886	1.901	1.882
O1-O2		2.794(33)	2.907(17)	2.895(26)	2.951(35)	2.944(33)	2.836(33)	2.852(21)
O1-O2'		3.069(16)	3.051(11)	3.097(12)	3.081(17)	3.094(18)	3.142(20)	3.193(16)
O2-O2'		3.065(17)	3.096(12)	3.103(13)	3.084(18)	3.096(19)	3.137(22)	3.198(18)
$<O_{bas}$-$O_{bas}>$		2.976	3.018	3.032	3.039	3.045	3.038	3.081
M1-O3	x4	2.016(19)	2.024(12)	1.952(16)	1.940(20)	1.967(20)	1.947(24)	2.026(19)
M1-O4	x2	1.919(36)	1.882(18)	2.125(25)	2.129(35)	2.049(33)	2.037(39)	2.185(24)
<M1-O>		1.984	1.977	2.010	2.003	1.994	1.977	2.079
M2-O3	x2	1.978(19)	1.969(13)	1.856(16)	1.839(20)	1.872(21)	1.828(24)	1.904(19)
M2-O3	x2	2.050(22)	2.020(11)	2.166(18)	2.170(24)	2.133(24)	2.180(28)	2.214(19)
M2-O4	x2	2.032(19)	2.040(10)	1.986(13)	1.980(19)	1.980(18)	1.955(19)	2.018(12)
<M2-O>		2.020	2.010	2.003	1.996	2.004	1.988	2.045
<M1,2-O>		2.008	1.999	2.005	1.998	2.001	1.984	2.056
I-O2	x4	2.258(18)	2.215(12)	2.113(16)	2.102(19)	2.183(21)	2.159(23)	2.084(16)
I-O1	x2	2.321(33)	2.296(14)	2.373(23)	2.369(32)	2.256(33)	2.321(37)	2.476(23)
$<I-O_{inner}>$		2.279	2.242	2.200	2.191	2.207	2.213	2.215

I-O2	x4	3.697(18)	3.724(11)	3.842(15)	3.847(21)	3.755(22)	3.700(23)	3.887(17)
I-O1	x2	3.770(36)	3.770(17)	3.591(29)	3.581(37)	3.794(38)	3.801(40)	3.641(25)
<I-O_{outer}>		3.721	3.739	3.758	3.758	3.768	3.734	3.805
Selected bond-angles ( )								
□O1-T-O3		106.1(10)	108.0(7)	107.4(8)	109.0(11)	107.0(11)	105.5(12)	105.9(9)
□O2-T-O3		108.1(10)	109.2(4)	110.8(7)	112.6(10)	113.3(10)	117.0(11)	114.1(8)
□O2'-T-O3		110.1(7)	110.3(5)	109.0(6)	109.5(8)	109.3(8)	108.8(9)	108.7(7)
mean = *t* (°)†		108.1	109.2	109.1	110.4	109.9	110.4	109.6
□O1–O2ə–O2	x2	62.0(9)	60.4(6)	58.9(6)	58.8(8)	59.0(8)	60.8(9)	59.0(7)
□O1-O2-O1		61.9(10)	60.2(6)	58.6(7)	58.7(8)	58.7(8)	60.4(10)	58.6(8)
mean		62.0	60.3	58.8	58.8	58.9	60.7	58.9
□O1-O2-O2'	x2	177.1(6)	177.0(5)	176.4(6)	177.1(8)	175.8(8)	174.8(9)	173.8(6)
□O2'-O1-O2'		170.7(13)	173.7(6)	176.0(10)	177.2(12)	174.7(13)	169.2(14)	170.8(9)
mean		175.0	175.9	176.3	177.1	175.4	172.9	172.8
Calculated parameters								
a (°)*		28.3	28.9	29.4	29.6	29.1	28.1	28.5
y_{M1}(°)‡		59.3	60.3	60.6	61.3	61.2	62.3	59.9
y_{M2}(°)		59.9	60.8	60.5	61.2	61.4	62.5	59.3
$(y_{M1}+2y_{M2})/3$		59.7	60.6	60.5	61.2	61.3	62.4	59.5
Sheet thicknesses (Å)								
tetrahedral t_t (Å)		2.407	2.453	2.485	2.519	2.515	2.535	2.509
octahedral t_o (Å)		2.026	1.959	1.972	1.926	1.920	1.837	2.088
interlayer separation t_i (Å)		2.806	2.797	2.746	2.748	2.779	2.866	2.702
D(Å)		1.790	1.974	1.997	2.051	2.059	2.107	1.950

* *a* (tetrahedral rotation angle) = $S_{i=1}^{6}$ I120 -f_iI/2 and where f_i is the angles between basal oxygens (Alietti et al. 1997).

†Tetrahedral flattening angle = mean O_{basal}-T-O_{apical}.

‡ $\cos\psi = t_o/(2d_o)$, $t_o = 2\{0.5-[2z_{O3}+z_{O4}]/3\}c\sin\beta$, d_o = <M-O> (Hazen and Burnham 1973).

§Sheet thickness $t_t = 4d_t/3$, $t_l = c\sin\beta - 2d_o\cos\psi - (8/3)d_t$, d_t = <T-O> (Donnay et al. 1964).

¶ Dimensional misfit between tetrahedral and octahedral sheets defined as $D = \{2\ \ 3\langle O_{bas}\text{-}O_{bas}\rangle - 3\ \ 2[(\langle M1\text{-}O\rangle + 2\langle M2\text{-}O\rangle)/3]$

885	**887**	**888**	**886**	**902**	**903**	**915**	**916**
$Si_{0.5}Ge_{0.5}HCln$	$Ni_1SiHCln$	$Ni_2SiHCln$	GeHCln	$Ga_1GeHCln$	$Ga_2GeHCln$	$Ga_3GeHCln$	$Ga_4GeHCln$
710–225	710–225	710–225	710–225	730–201	730–201	715–210	715–210
1.815(19)	1.823(16)	1.778(23)	1.828(39)	1.725(9)	1.864(15)	1.744(11)	1.797(32)
1.785(27)	1.702(23)	1.779(33)	1.722(55)	1.996(21)	1.805(16)	2.077(22)	1.892(66)
1.857(19)	1.915(17)	2.011(25)	1.929(41)	1.795(14)	1.902(14)	1.825(16)	1.926(45)
1.807(14)	1.758(10)	1.758(15)	1.874(24)	1.864(11)	1.874(10)	1.910(12)	1.956(28)
1.816	1.800	1.832	1.838	1.845	1.861	1.889	1.893
2.937(34)	2.824(30)	2.860(41)	2.919(57)	2.895(21)	3.018(23)	2.981(24)	2.953(54)
3.018(17)	3.039(13)	3.161(19)	3.008(31)	3.030(16)	3.017(15)	3.089(17)	3.140(37)
3.020(17)	3.037(14)	3.160(23)	3.005(30)	3.026(15)	3.015(14)	3.088(18)	3.140(38)
2.992	2.967	3.060	2.977	2.984	3.017	3.053	3.078
2.016(21)	2.068(17)	2.081(21)	2.036(38)	2.003(15)	2.072(16)	1.992(18)	2.034(40)
2.007(29)	1.855(32)	2.158(36)	1.903(67)	2.218(20)	1.991(21)	2.254(23)	2.092(64)
2.013	1.997	2.107	1.992	2.075	2.045	2.079	2.053
1.936(21)	2.015(17)	2.095(22)	1.942(38)	1.864(18)	1.965(17)	1.861(17)	1.928(38)
2.131(26)	2.019(22)	2.074(26)	1.935(44)	2.126(16)	2.003(17)	2.168(19)	2.026(47)
2.003(20)	2.072(17)	2.116(20)	2.073(36)	2.030(14)	2.083(14)	2.027(13)	2.121(33)
2.023	2.035	2.095	1.983	2.007	2.017	2.019	2.025
2.020	2.022	2.099	1.986	2.030	2.026	2.039	2.034
2.282(17)	2.264(14)	2.142(21)	2.275(33)	2.206(15)	2.296(12)	2.159(17)	2.246(40)
2.233(31)	2.240(28)	2.093(36)	2.346(67)	2.498(19)	2.270(21)	2.492(23)	2.382(65)
2.266	2.256	2.126	2.299	2.303	2.287	2.270	2.291

3.690(19)	3.658(15)	3.710(23)	3.694(39)	3.799(16)	3.705(15)	3.891(16)	3.851(42)
3.822(35)	3.782(32)	3.892(39)	3.772(65)	3.569(20)	3.863(22)	3.604(24)	3.807(66)
3.734	3.699	3.771	3.720	3.722	3.758	3.795	3.836
107.0(10)	107.7(8)	107.8(13)	107.2(16)	108.9(9)	109.3(7)	108.8(9)	108.2(18)
110.2(12)	108.7(11)	104.3(14)	113.1(17)	111.6(7)	110.7(7)	112.8(7)	107.7(17)
107.5(8)	110.7(7)	111.3(9)	108.6(14)	109.3(6)	110.0(6)	108.4(6)	108.6(14)
108.2	109.0	107.8	109.6	109.9	110.0	110.0	108.2
61.4(8)	62.0(8)	55.8(11)	63.2(15)	63.6(7)	62.1(6)	60.7(7)	60.0(14)
61.3(9)	62.0(9)	55.5(11)	63.1(16)	63.7(7)	62.0(6)	60.8(7)	59.8(15)
61.4	62.0	55.7	63.2	63.6	62.1	60.7	59.9
178.6(6)	178.0(6)	171.7(10)	176.4(14)	176.8(8)	177.0(6)	178.0(7)	177.1(16)
175.8(13)	172.5(12)	172.7(13)	172.6(25)	172.2(8)	174.9(9)	175.3(9)	174.4(22)
177.7	176.2	172.0	175.1	175.3	176.3	177.1	176.2
29.1	28.6	29.1	28.0	27.9	28.6	29.1	29.1
59.5	58.5	55.4	61.6	60.8	60.3	61.1	61.3
59.7	59.1	55.2	61.4	59.8	59.9	60.2	60.8
59.6	58.9	55.3	61.5	60.1	60.0	60.5	61.0
2.421	2.400	2.443	2.451	2.460	2.481	2.519	2.524
2.044	2.089	2.393	1.897	2.022	1.994	2.008	1.973
2.800	2.762	2.367	2.910	2.819	2.839	2.791	2.844
1.794	1.699	1.695	1.887	1.724	1.856	1.925	2.033

} (Toraya 1981).

TABLE 5. OH- and OD-stretching bands for synthetic clintonites

Run no.		[875]	[894]	[876]	[895]	[877]	[878]	[879]	[885]	[887]	[888]	[907]	[908]	[909]	[886]	[902]	[903]	[915]	[916]	[944]	[945]	[946]
Symbol		SiHCln	$Ga_{0.5}$SiHCln	Ga_1SiHCln	$Ga_{1.5}$SiHCln	Ga_2SiHCln	Ga_3SiHCln	Ga_4SiHCln	$Si_{0.5}Ge_{2.5}$HCln	Ni_1SiHCln	Ni_2SiHCln	SiDCln	Ga2SiDCln	Ga4SiDCln	GeHCln	Ga1GeHCln	Ga2GeHCln	Ga3GeHCln	Ga4GeHCln	GeDCln	Ga2GeDCln	Ga4GeDCln
	Position (cm^{-1})	3741.8	3739.4	3733.1	3725.0	3724.6	3716.3	3709.3			3631.5	2756.7	2745.8	2736.7	3689.7	3676.7	3663.6	3649.4	3624.4	2719.5	2702.0	2679.0
N	FWHH (cm^{-1})*	25.3	27.9	24.6	32.4	27.8	26.2	23.4			32.6	24.7	23.0	19.1	41.9	37.6	48.4	61.5	88.6	31.9	36.4	56.4
	Intensity (%)†	0.4	0.4	0.4	0.5	0.9	0.5	0.5			2.1	2.2	1.5	1.1	3.3	1.8	1.9	5.1	7.4	6.1	3.7	8.2
	G/(G+L) (%)‡	100.0	100.0	0.0	100.0	0.0	100.0	100.0			100.0	86.2	100.0	100.0	100.0	100.0	100.0	100.0	79.6	100.0	100.0	100.0
	Position (cm^{-1})	3686.5	3675.6	3657.1	3649.3	3655.7	3652.1	3644.4	3686.8	3631.5	3604.5	2724.7	2708.7	2689.1	3618.0	3612.9	3593.1	3583.9	3524.0	2678.9	2661.1	2632.9
I_A	FWHH (cm^{-1})	80.8	88.5	95.5	99.7	89.4	83.1	78.0	59.2	90.0	58.2	37.7	46.0	56.9	72.1	71.9	85.2	76.5	81.7	42.6	49.7	41.0
	Intensity (%)	9.4	10.3	12.6	15.8	15.6	10.6	11.0	6.1	20.9	9.5	10.3	12.6	21.1	31.4	15.5	16.2	13.7	30.2	27.1	14.6	11.0
	G/(G+L) (%)	100.0	100.0	100.0	100.0	100.0	100.0	55.7	100.0	78.2	100.0	100.0	100.0	68.4	100.0	100.0	100.0	100.0	88.2	92.1	100.0	100.0
	Position (cm^{-1})	3618.5	3605.7	3588.2	3578.6	3589.6	3590.1	3592.3	3618.7	3577.6	3548.5	2691.8	2674.1	2652.1	3671.0	3573.4	3554.9	3543.0	3454.7	2660.5	2634.8	2605.5
I_B	FWHH (cm^{-1})	100.9	108.1	109.8	119.6	101.9	99.0	83.9	84.5	100.0	82.0	49.5	51.4	44.2	115.2	94.8	114.8	103.1	101.2	49.2	61.4	51.8
	Intensity (%)	37.2	42.1	36.7	39.2	30.9	25.6	18.4	49.9	36.2	27.8	26.8	24.0	15.7	49.3	37.9	43.8	42.4	31.5	38.3	41.0	33.2
	G/(G+L) (%)	100.0	100.0	100.0	100.0	100.0	100.0	68.3	100.0	100.0	92.6	100.0	100.0	100.0	69.3	80.1	77.9	74.8	64.2	100.0	83.5	76.4
	Position (cm^{-1})	3558.4	3537.5	3518.6	3504.6	3531.6	3529.9	3529.0	3565.4	3520.0	3490.2	2659.8	2638.0	2620.0	3436.5	3519.8	3687.8	3470.2	3387.1	2626.5	2594.3	2558.4
I_C	FWHH (cm^{-1})	135.9	136.1	135.1	150.9	128.5	105.1	96.2	103.2	123.7	112.1	57.7	56.6	44.5	151.7	125.5	134.4	123.4	136.4	63.5	82.6	77.9
	Intensity (%)	39.1	33.1	29.8	25.7	33.5	34.4	33.6	32.3	28.2	33.0	44.3	26.9	18.9	16.1	29.8	25.1	25.3	13.7	25.3	30.9	47.7
	G/(G+L) (%)	89.2	100.0	80.9	100.0	62.6	76.9	100.0	85.2	100.0	48.3	100.0	100.0	100.0	100.0	73.6	99.0	100.0	100.0	86.5	69.4	0.0
	Position (cm^{-1})	3422.9	3413.8	3417.9	3412.3	3435.6	3453.7	3446.5	3443.9	3409.6	3415.4	2620.0	2600.9	2592.9		3418.0		3384.7	3562.9		2519.7	
I_D	FWHH (cm^{-1})	144.3	141.2	159.3	184.0	159.2	120.1	110.5	149.5	142.0	199.2	63.6	86.4	50.2		156.8		145.7	82.8		110.1	
	Intensity (%)	14.0	14.2	20.5	18.9	19.1	19.8	24.8	11.7	14.7	27.6	15.9	35.0	17.9		15.1		13.5	17.2		9.8	
	G/(G+L) (%)	100.0	100.0	100.0	100.0	100.0	100.0	84.9	100.0	100.0	100.0	100.0	23.8	66.9		100.0		100.0	37.3		100.0	
	Position (cm^{-1})						3374.0	3770.4						2552.2								
I_E	FWHH (cm^{-1})						136.9	142.2						74.0								
	Intensity (%)						9.1	11.8						25.2								
	G/(G+L) (%)						100.0	100.0						29.4								
	Position (cm^{-1})											2510.6								2508.3		
V	FWHH (cm^{-1})											33.1								84.4		
	Intensity (%)											0.6								3.2		
	G/(G+L) (%)											95.6								0.0		

* Full-width at half-maximum height.
† Areal intensity ratio as total = 100 %.
‡ G = Gaussian component. L = Lorentzian component.

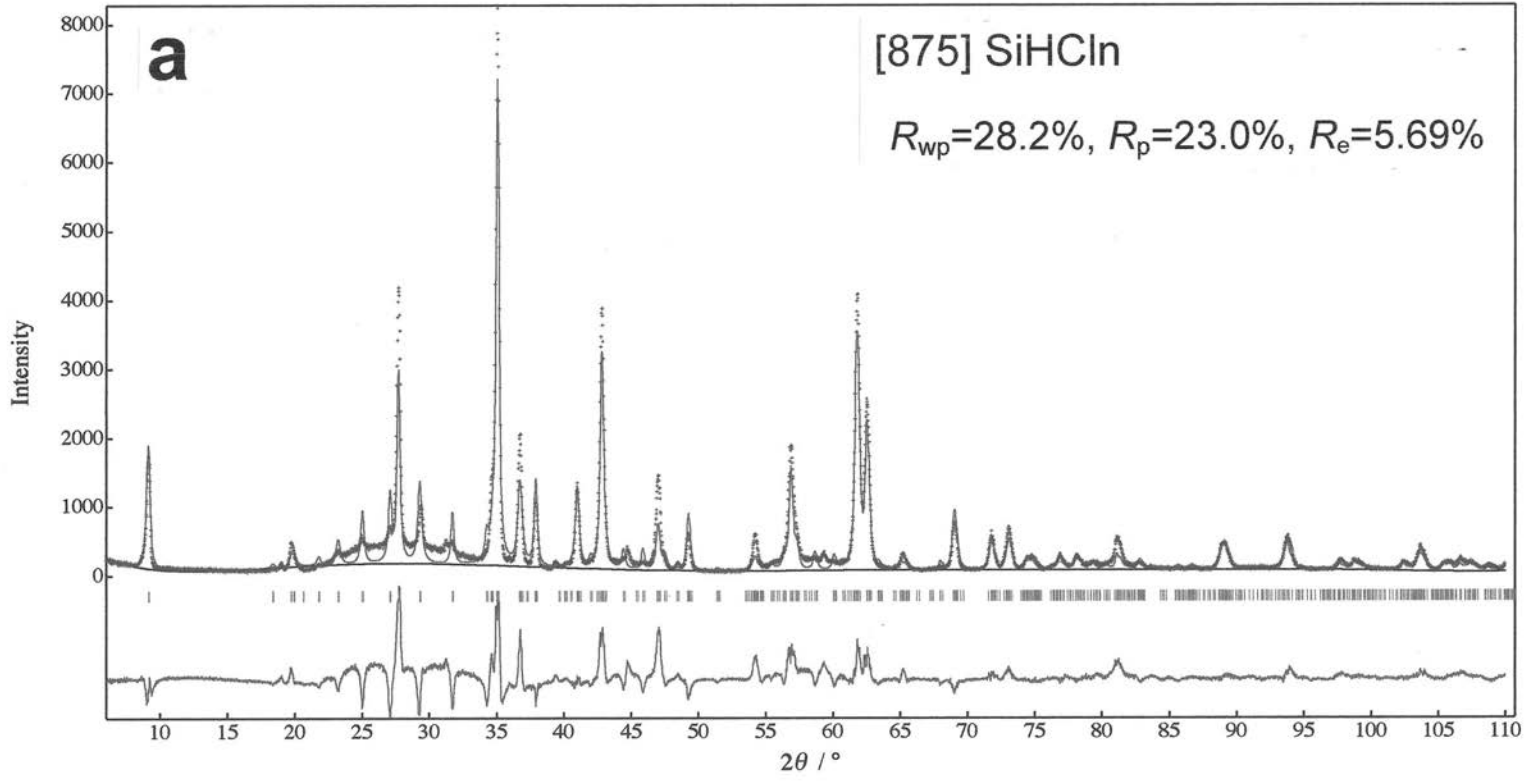
a
[875] SiHCln
R_{wp}=28.2%, R_p=23.0%, R_e=5.69%
Intensity
8000
7000
6000
5000
4000
3000
2000
1000
0
10 15 20 25 30 35 40 45 50 55 60 65 70 75 80 85 90 95 100 105 110
2θ / °

Fig. 1a

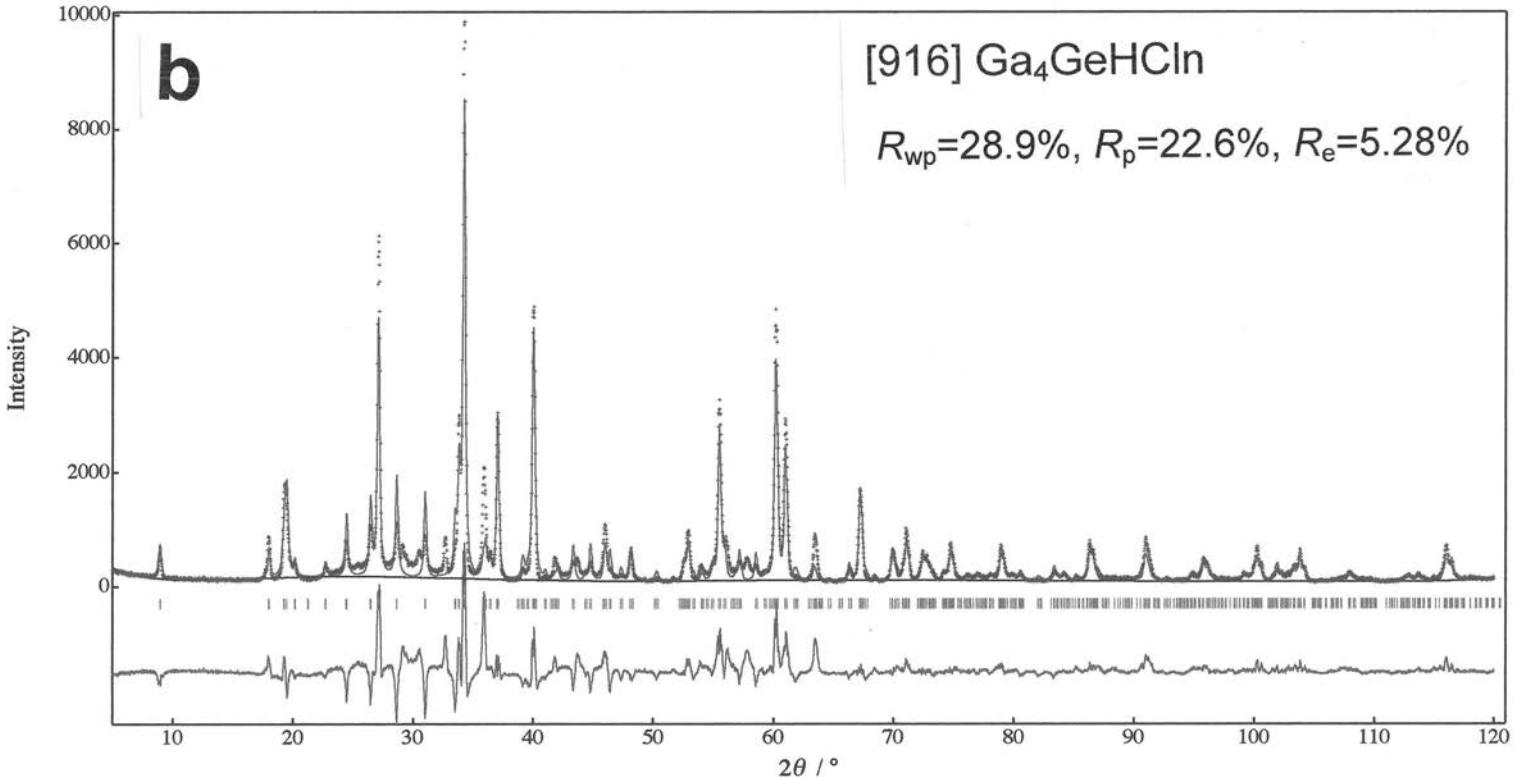
b
[916] Ga4GeHCln
Rwp=28.9%, Rp=22.6%, Re=5.28%
Intensity
10000
8000
6000
4000
2000
0
10
20
30
40
50
60
70
80
90
100
110
120
2θ / °

Fig.16

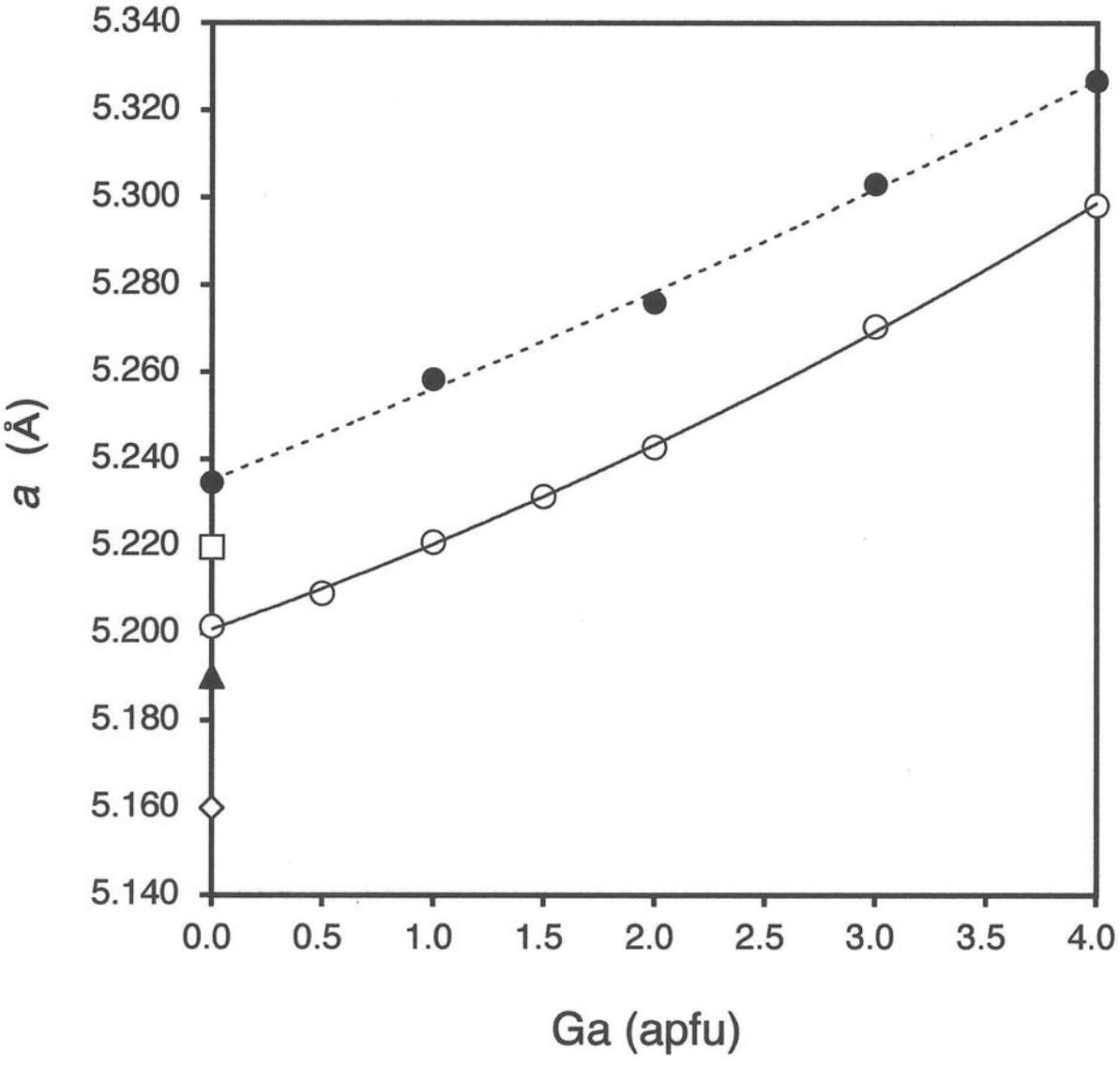
5.340
5.320
5.300
5.280
5.260
5.240
5.220
5.200
5.180
5.160
5.140
a (Å)
0.0
0.5
1.0
1.5
2.0
2.5
3.0
3.5
4.0
Ga (apfu)

Fig. 2a

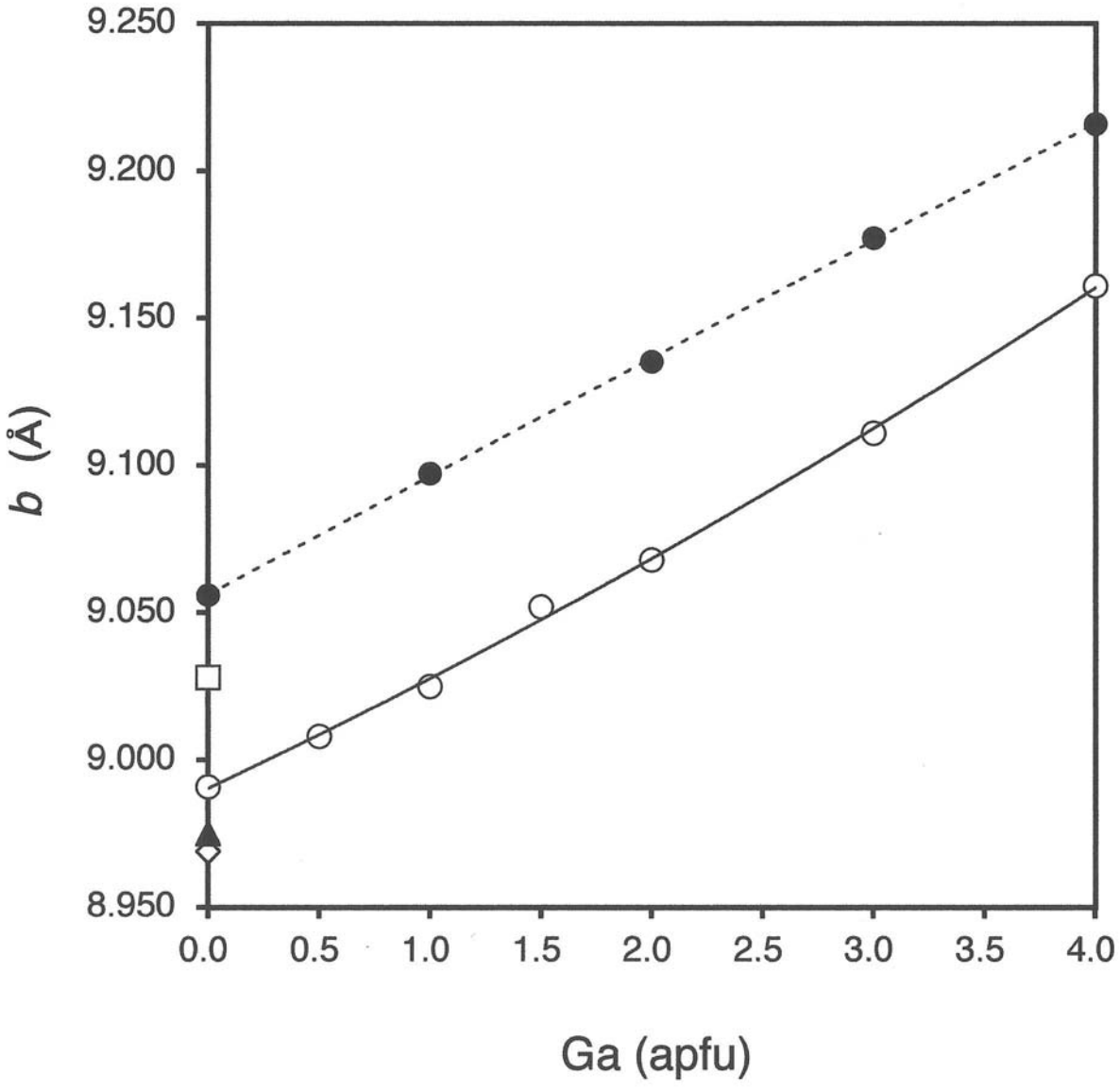
9.250
9.200
9.150
9.100
9.050
9.000
8.950
b (Å)
0.0
0.5
1.0
1.5
2.0
2.5
3.0
3.5
4.0
Ga (apfu)

Fig.2b

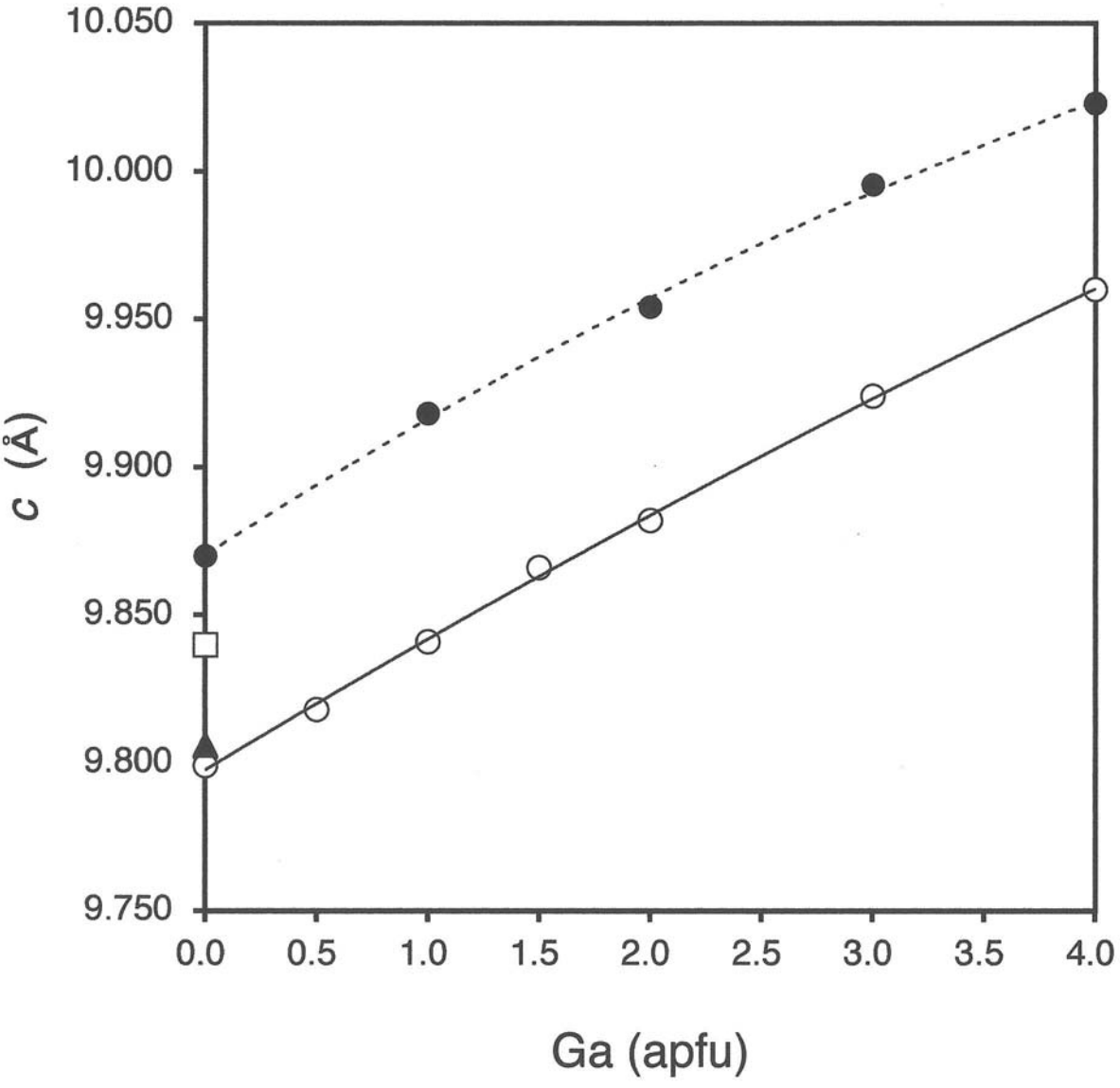
10.050
10.000
9.950
9.900
9.850
9.800
9.750
c (Å)
0.0
0.5
1.0
1.5
2.0
2.5
3.0
3.5
4.0
Ga (apfu)

Fig.2c

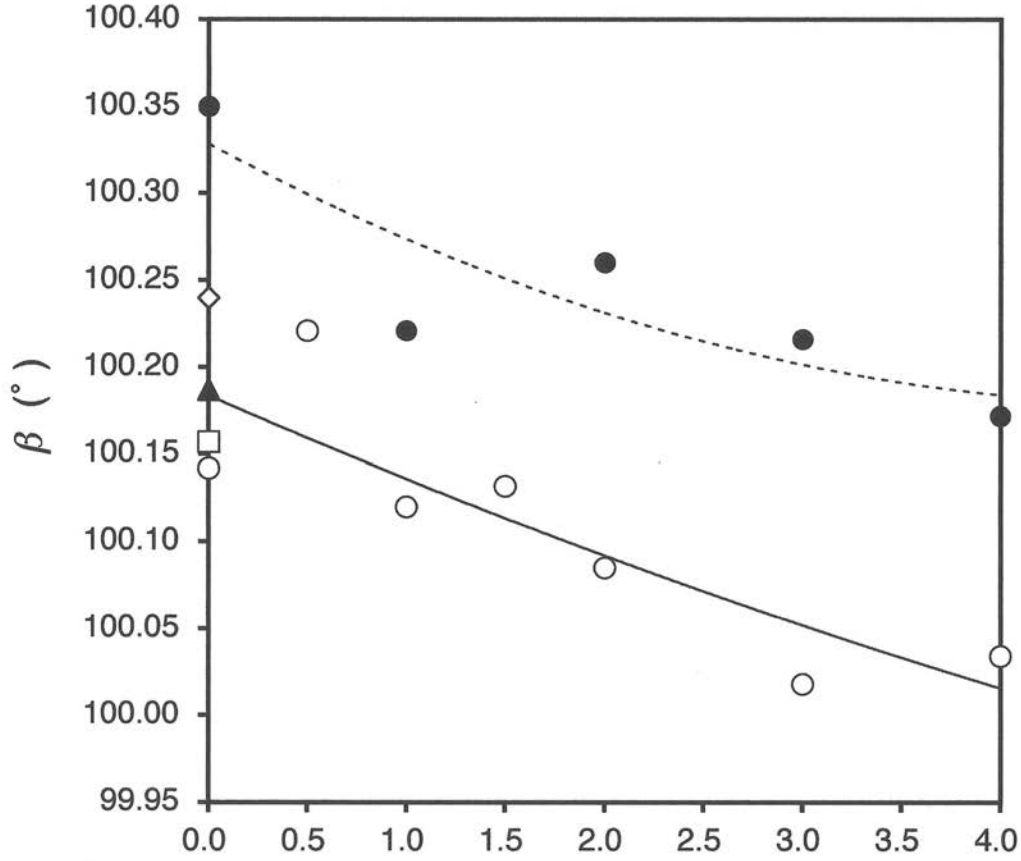
100.40
100.35
100.30
100.25
100.20
100.15
100.10
100.05
100.00
99.95
β (°)
0.0
0.5
1.0
1.5
2.0
2.5
3.0
3.5
4.0
Ga (apfu)

Fig. 2d

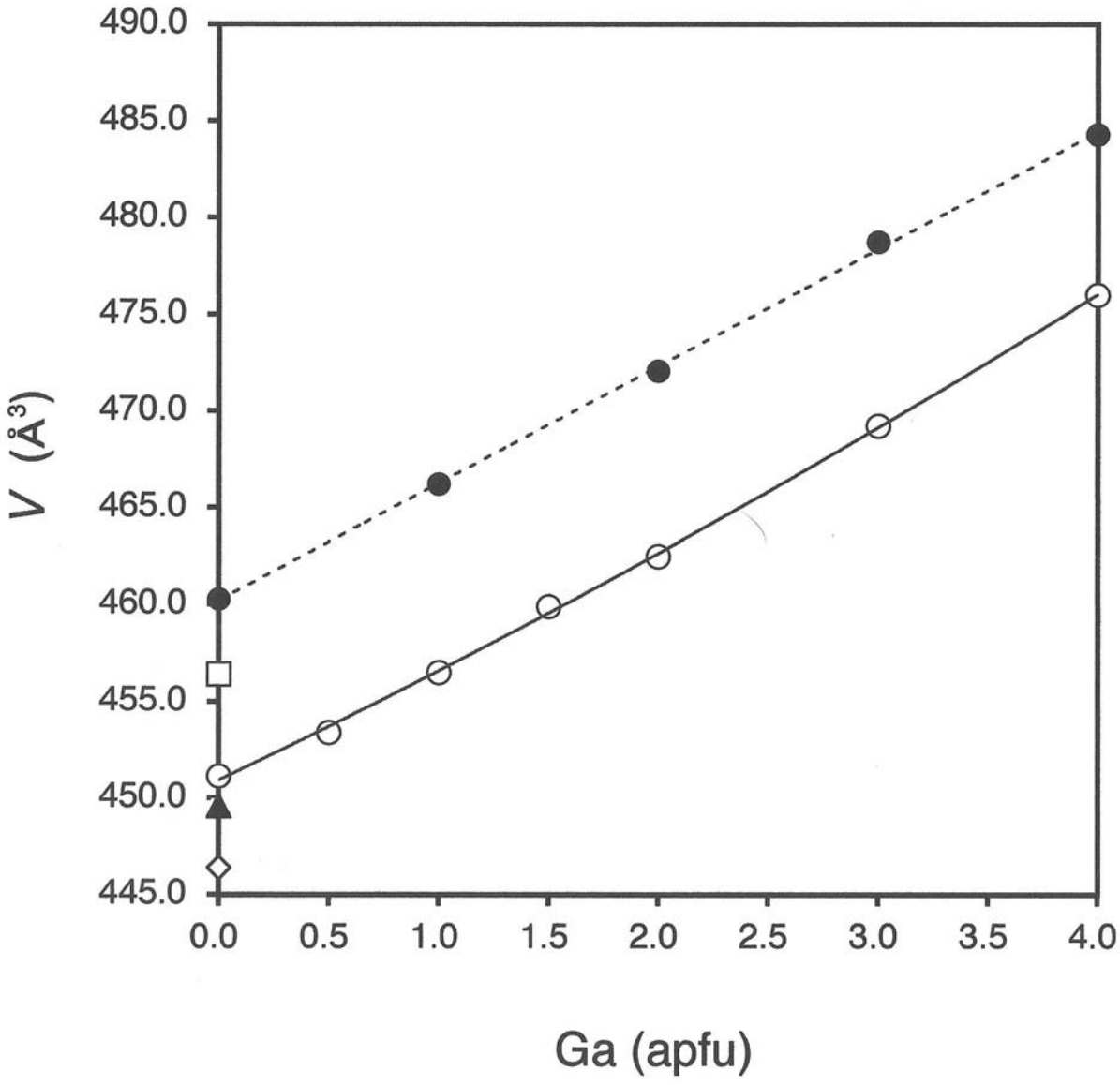
490.0
485.0
480.0
475.0
470.0
465.0
460.0
455.0
450.0
445.0
V (Å3)
0.0
0.5
1.0
1.5
2.0
2.5
3.0
3.5
4.0
Ga (apfu)

Fig.2e

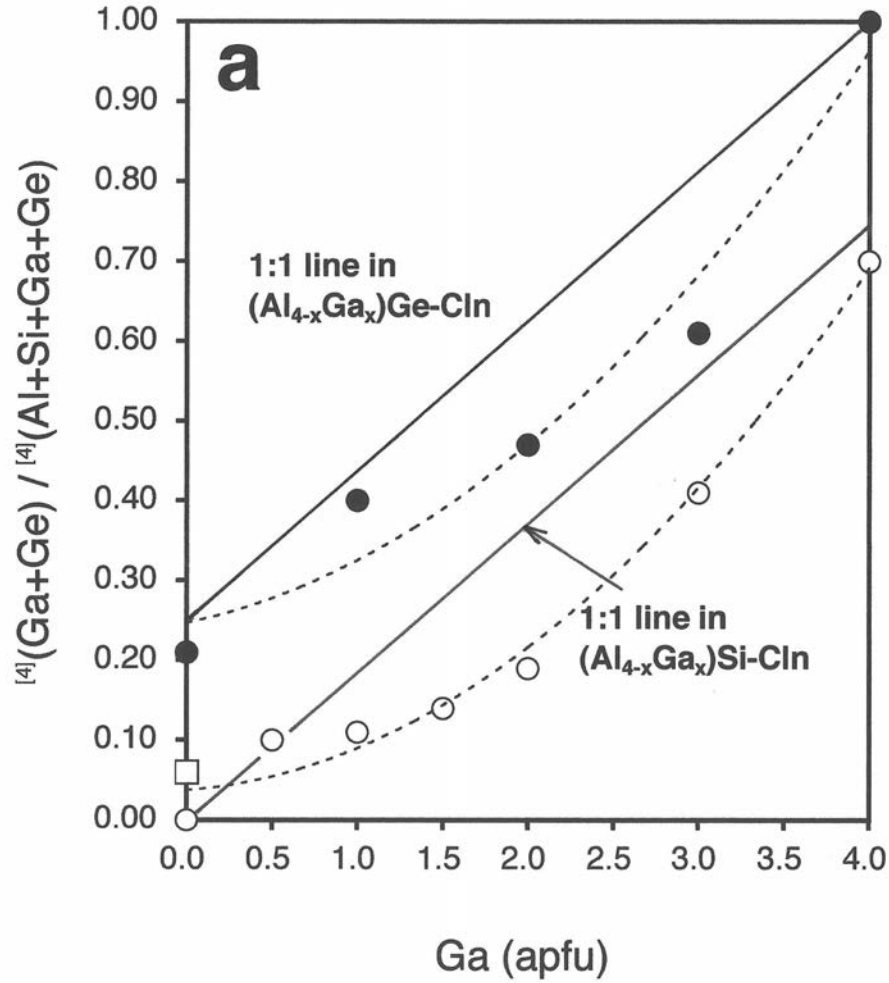
a
1.00
0.90
0.80
0.70
0.60
0.50
0.40
0.30
0.20
0.10
0.00
0.0
0.5
1.0
1.5
2.0
2.5
3.0
3.5
4.0
[4](Ga+Ge) / [4](Al+Si+Ga+Ge)
Ga (apfu)
1:1 line in
(Al4-xGax)Ge-Cln
1:1 line in
(Al4-xGax)Si-Cln

Fig.3a

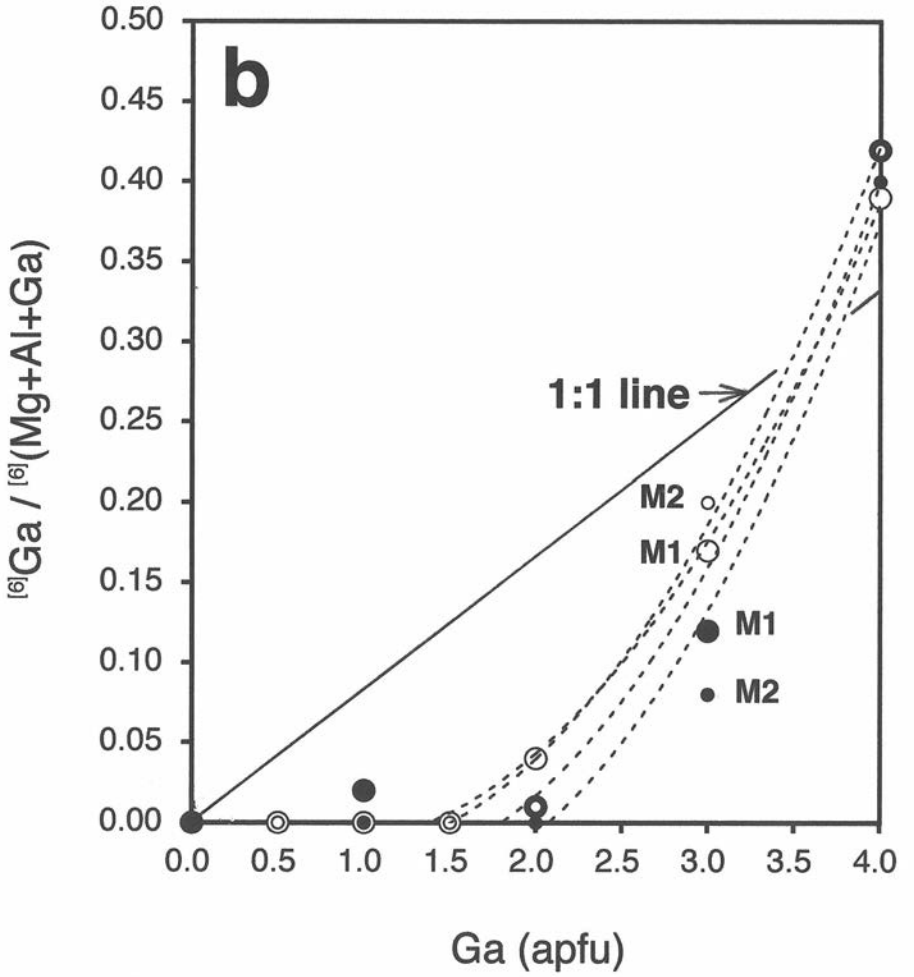
b
0.50
0.45
0.40
0.35
0.30
0.25
0.20
0.15
0.10
0.05
0.00
[6]Ga / [6](Mg+Al+Ga)
1:1 line
M2
M1
M1
M2
0.0
0.5
1.0
1.5
2.0
2.5
3.0
3.5
4.0
Ga (apfu)

Fig. 3b

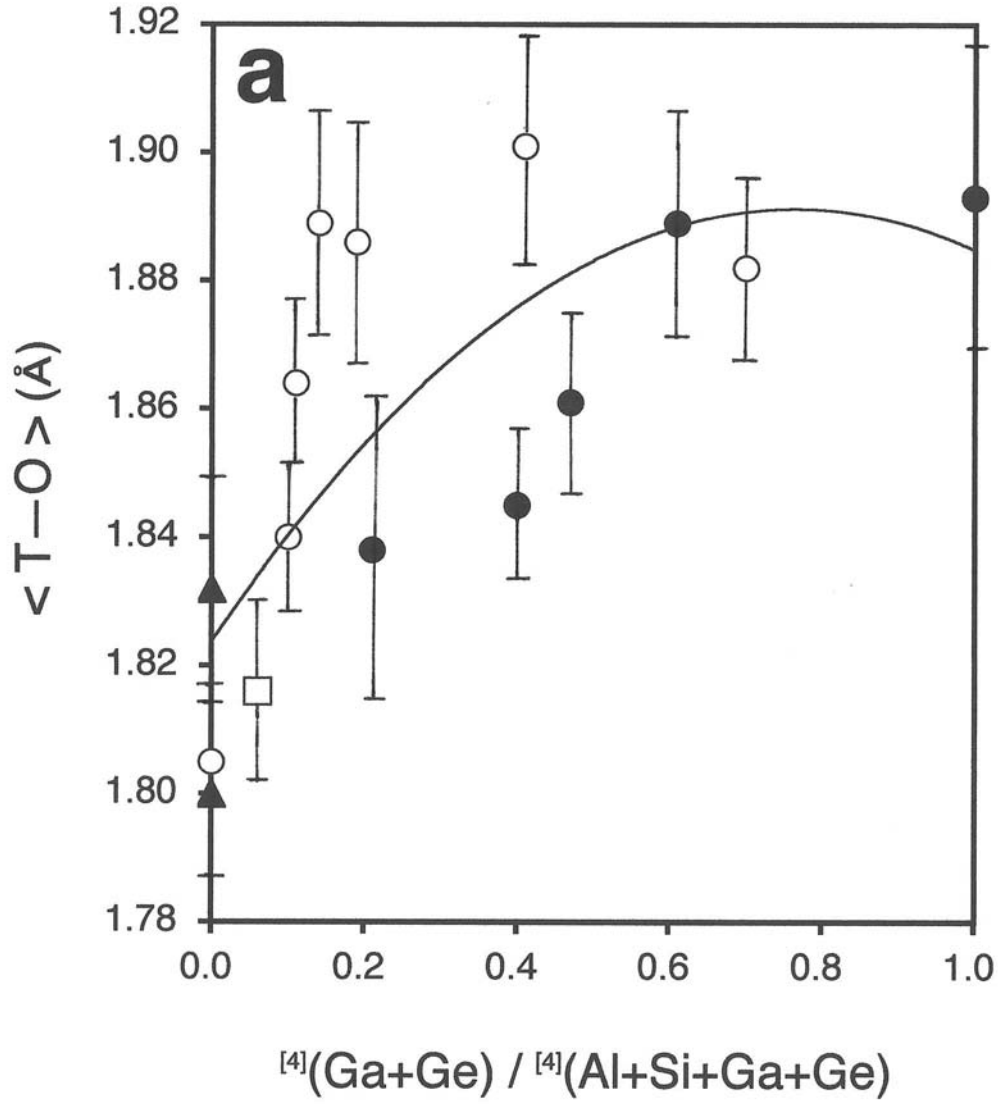
a
1.92
1.90
1.88
1.86
1.84
1.82
1.80
1.78
< T—O > (Å)
0.0
0.2
0.4
0.6
0.8
1.0
[4](Ga+Ge) / [4](Al+Si+Ga+Ge)

Fig. 4a

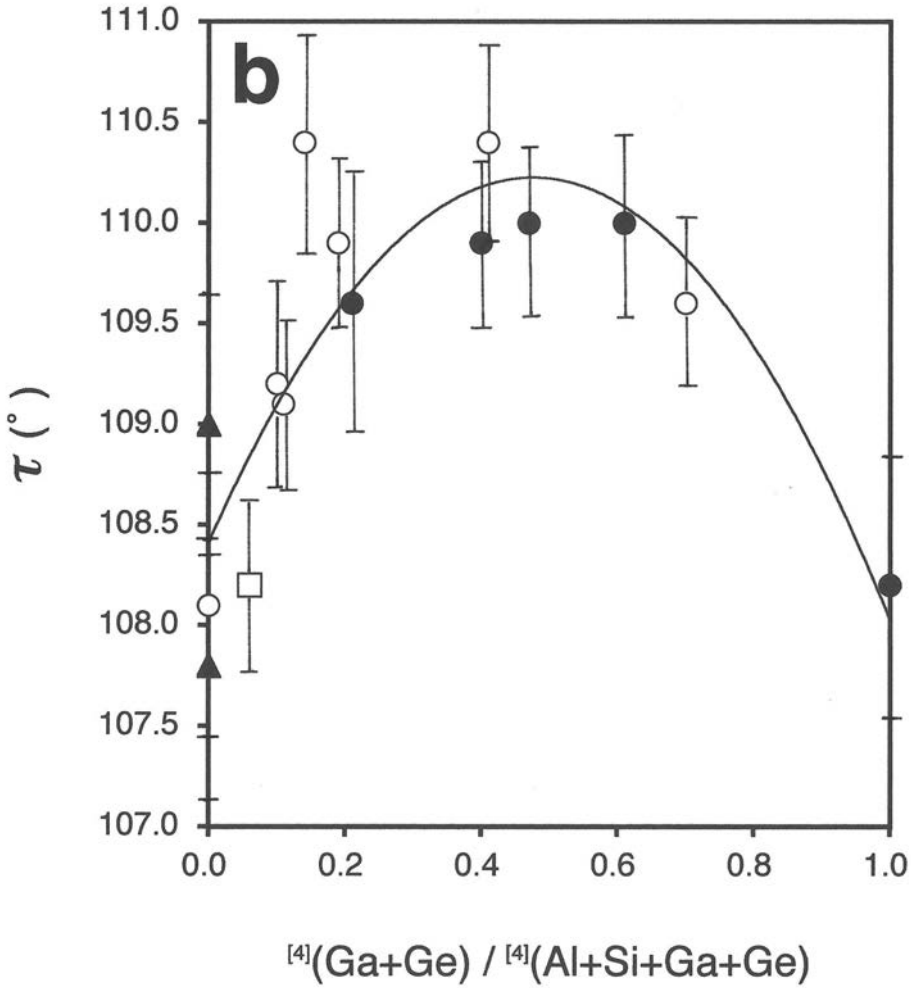
b
111.0
110.5
110.0
109.5
109.0
108.5
108.0
107.5
107.0
τ (°)
0.0
0.2
0.4
0.6
0.8
1.0
[4](Ga+Ge) / [4](Al+Si+Ga+Ge)

Fig. 4b

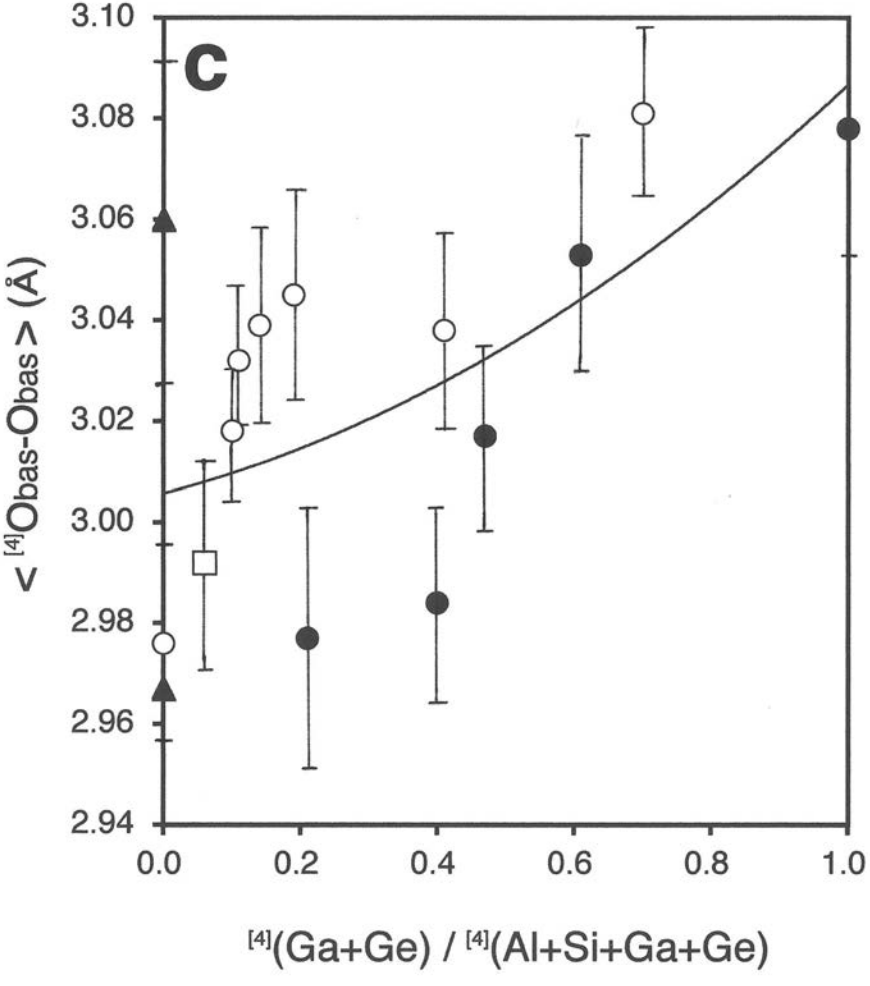
c
3.10
3.08
3.06
3.04
3.02
3.00
2.98
2.96
2.94
0.0
0.2
0.4
0.6
0.8
1.0
< [4]Obas-Obas > (Å)
[4](Ga+Ge) / [4](Al+Si+Ga+Ge)

Fig.4c

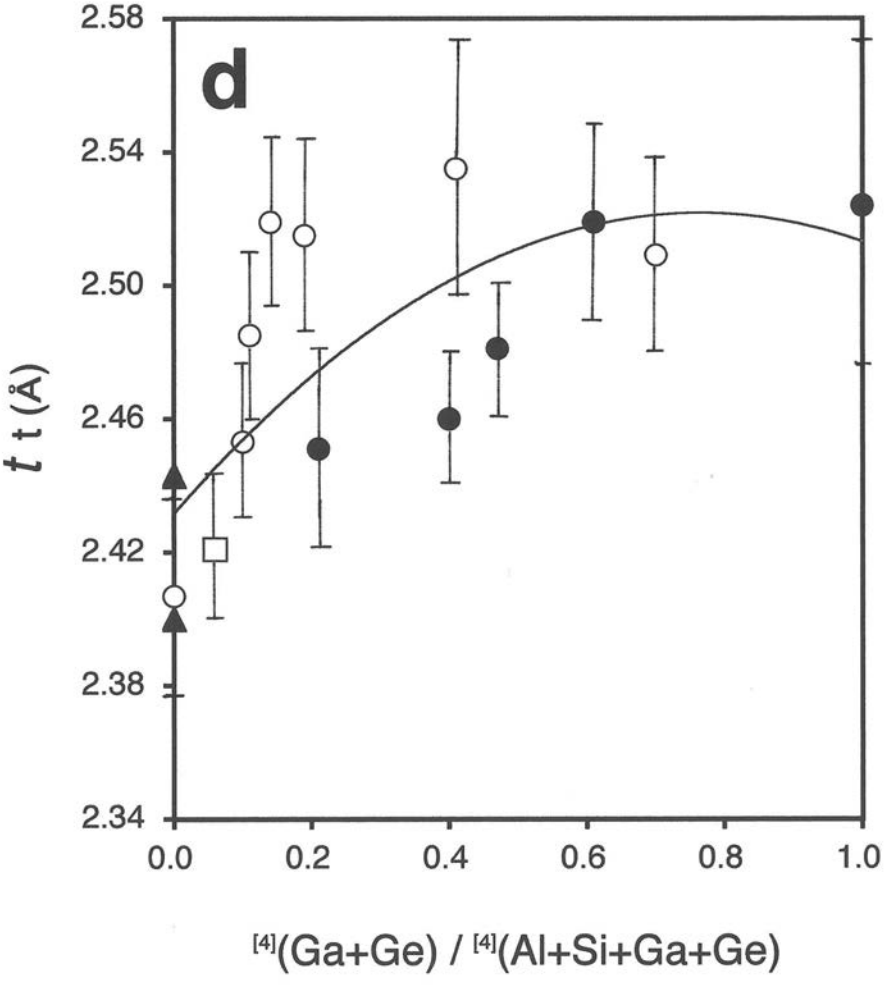
d
2.58
2.54
2.50
2.46
2.42
2.38
2.34
t t (Å)
0.0
0.2
0.4
0.6
0.8
1.0
[4](Ga+Ge) / [4](Al+Si+Ga+Ge)

Fig.4d

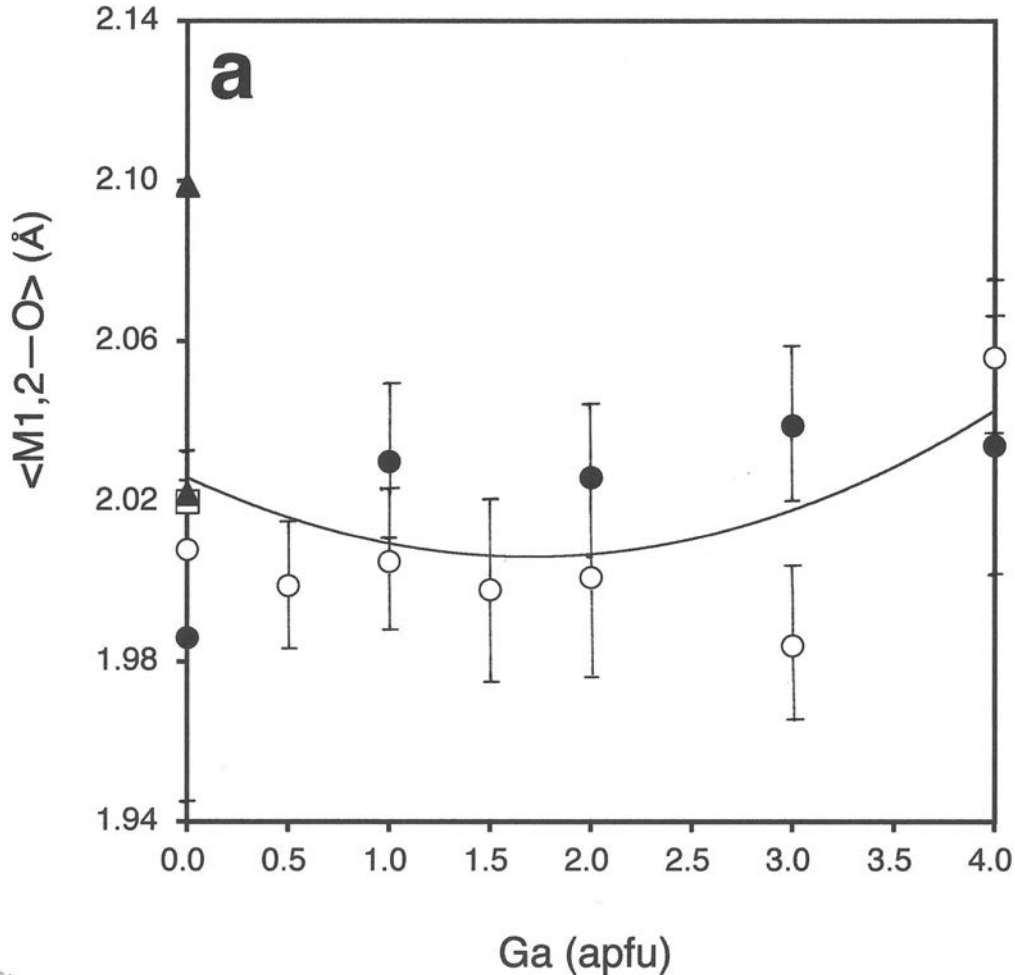

Fig.5a

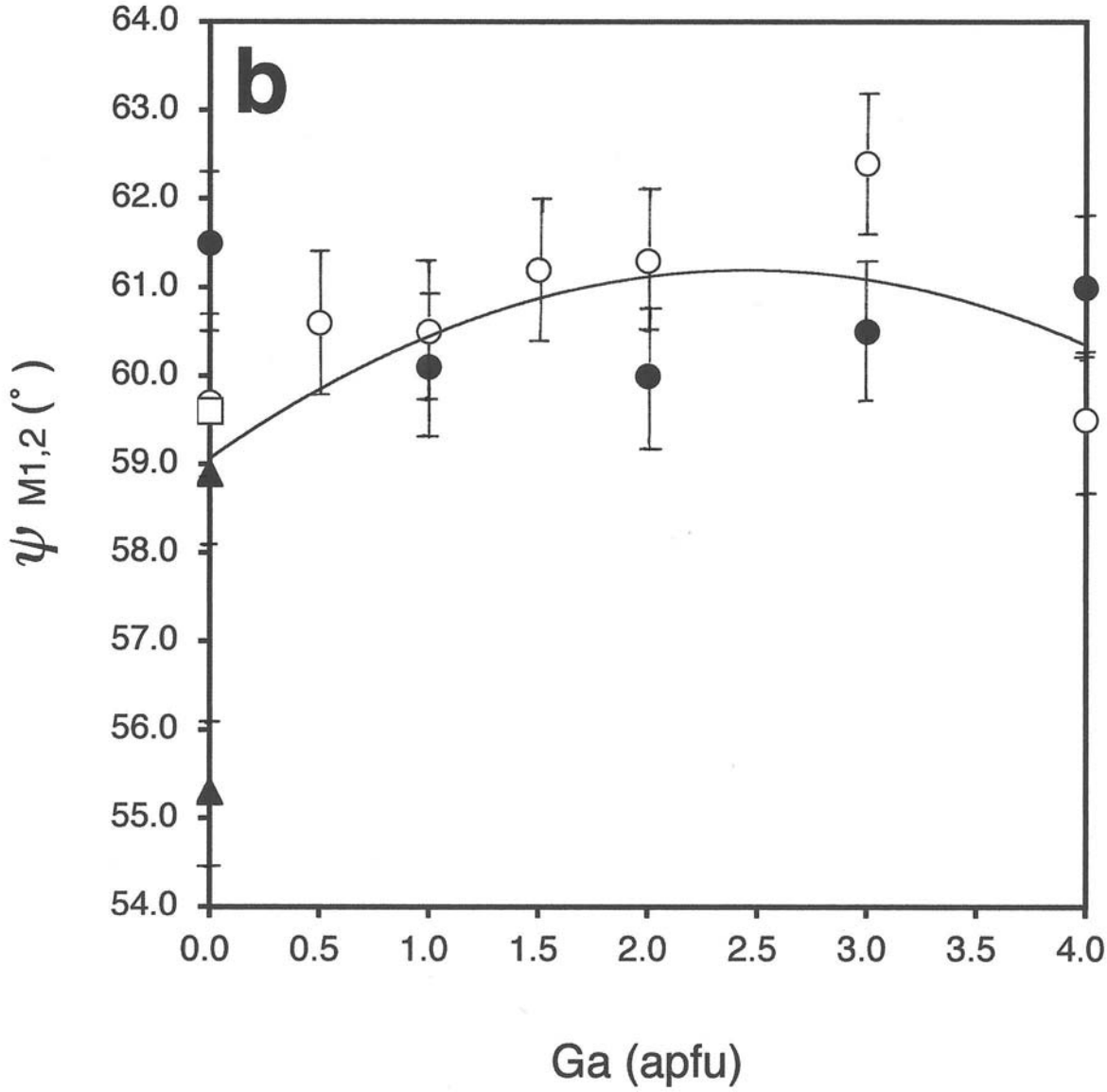
b
64.0
63.0
62.0
61.0
60.0
59.0
58.0
57.0
56.0
55.0
54.0
ψ M1,2 (°)
0.0
0.5
1.0
1.5
2.0
2.5
3.0
3.5
4.0
Ga (apfu)

Fig. 5b

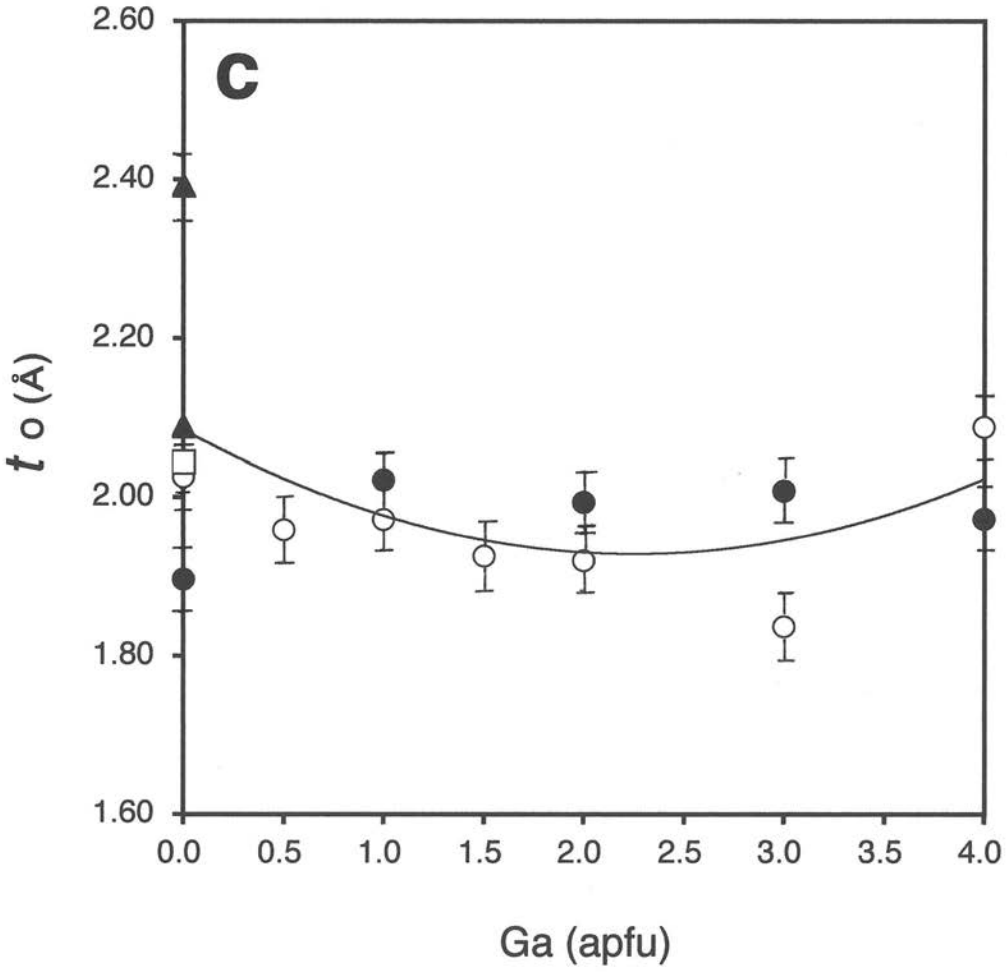

Fig5c

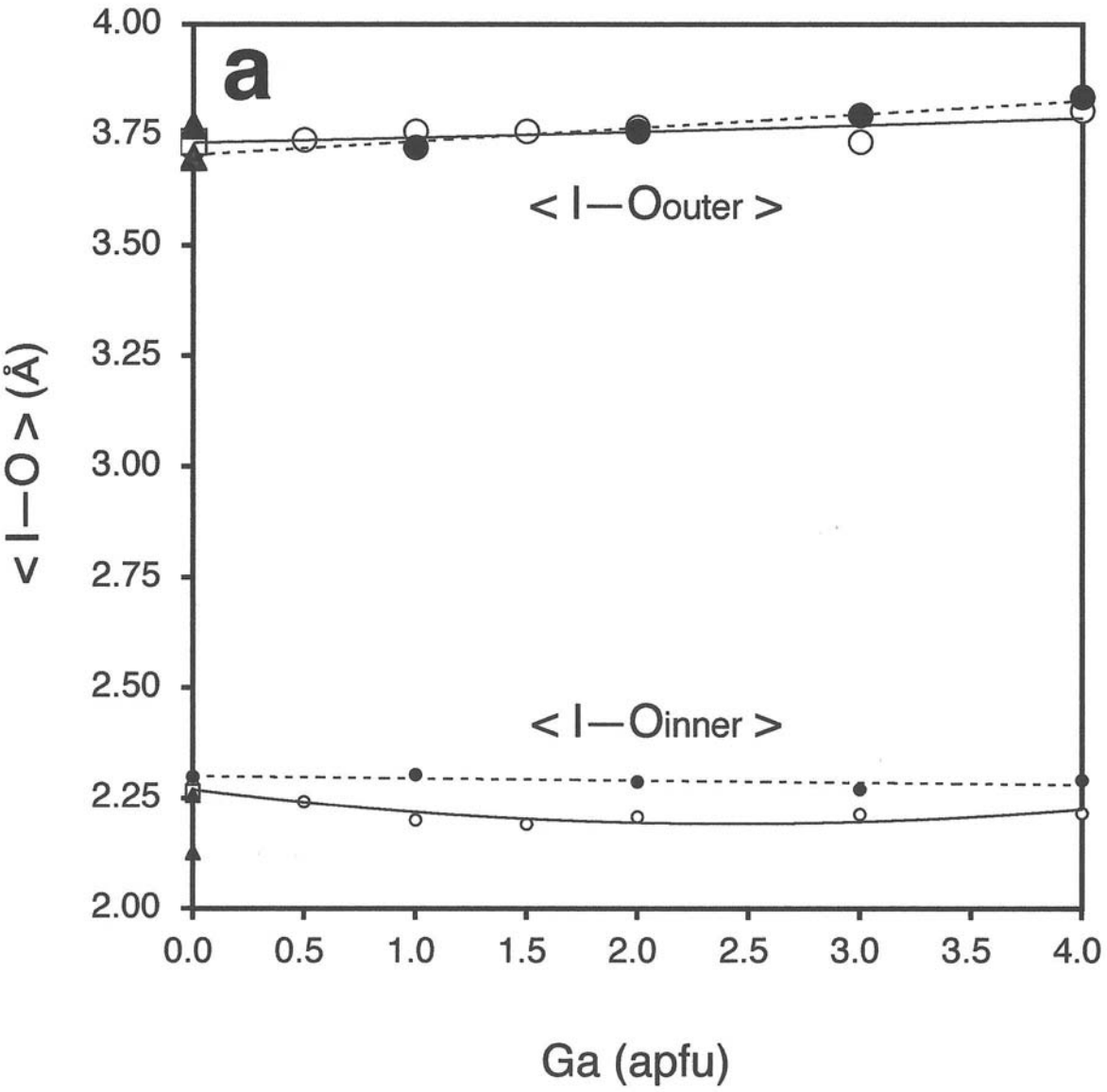
a
4.00
3.75
3.50
3.25
3.00
2.75
2.50
2.25
2.00
< I—Oouter >
< I—Oinner >
< I—O > (Å)
0.0
0.5
1.0
1.5
2.0
2.5
3.0
3.5
4.0
Ga (apfu)

Fig. 6a

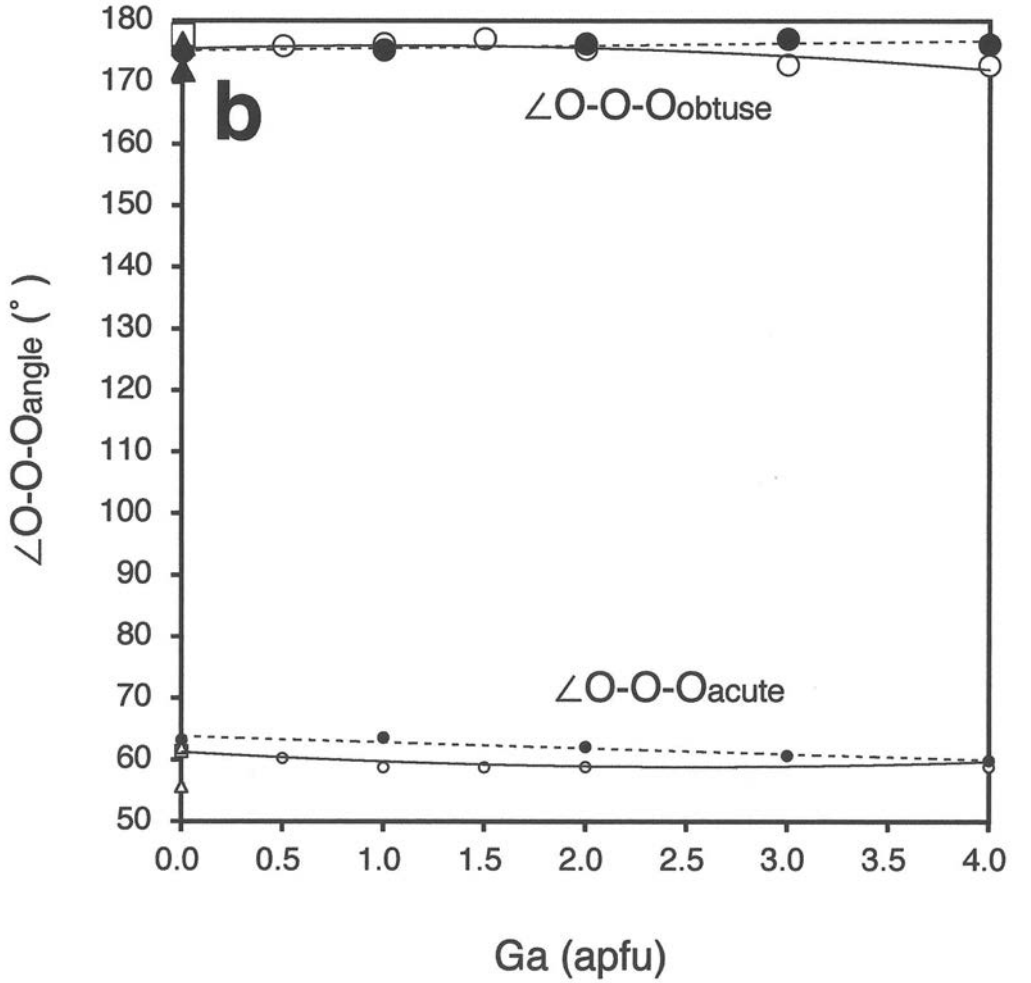
b
∠O-O-Oobtuse
∠O-O-Oacute
∠O-O-Oangle (°)
Ga (apfu)
180
170
160
150
140
130
120
110
100
90
80
70
60
50
0.0
0.5
1.0
1.5
2.0
2.5
3.0
3.5
4.0

Fig. 6b

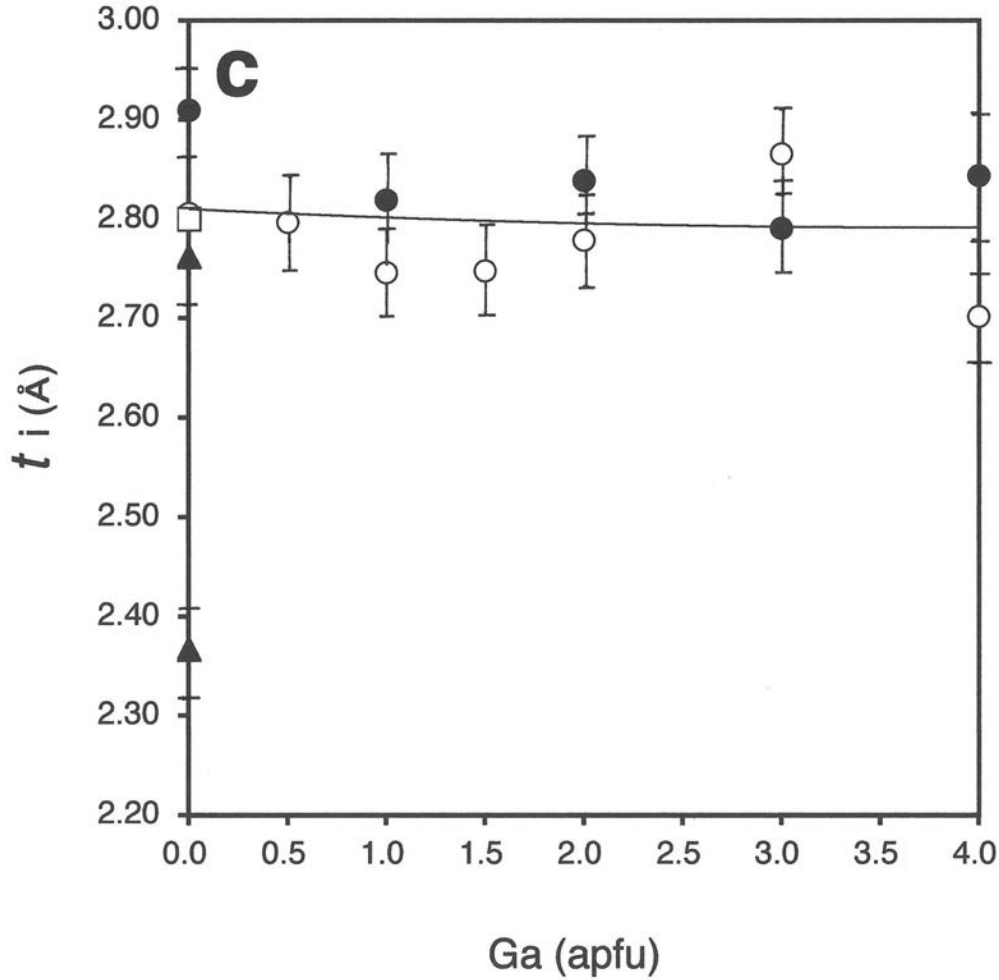
C
3.00
2.90
2.80
2.70
2.60
2.50
2.40
2.30
2.20
t i (Å)
0.0
0.5
1.0
1.5
2.0
2.5
3.0
3.5
4.0
Ga (apfu)

Fig. 6C

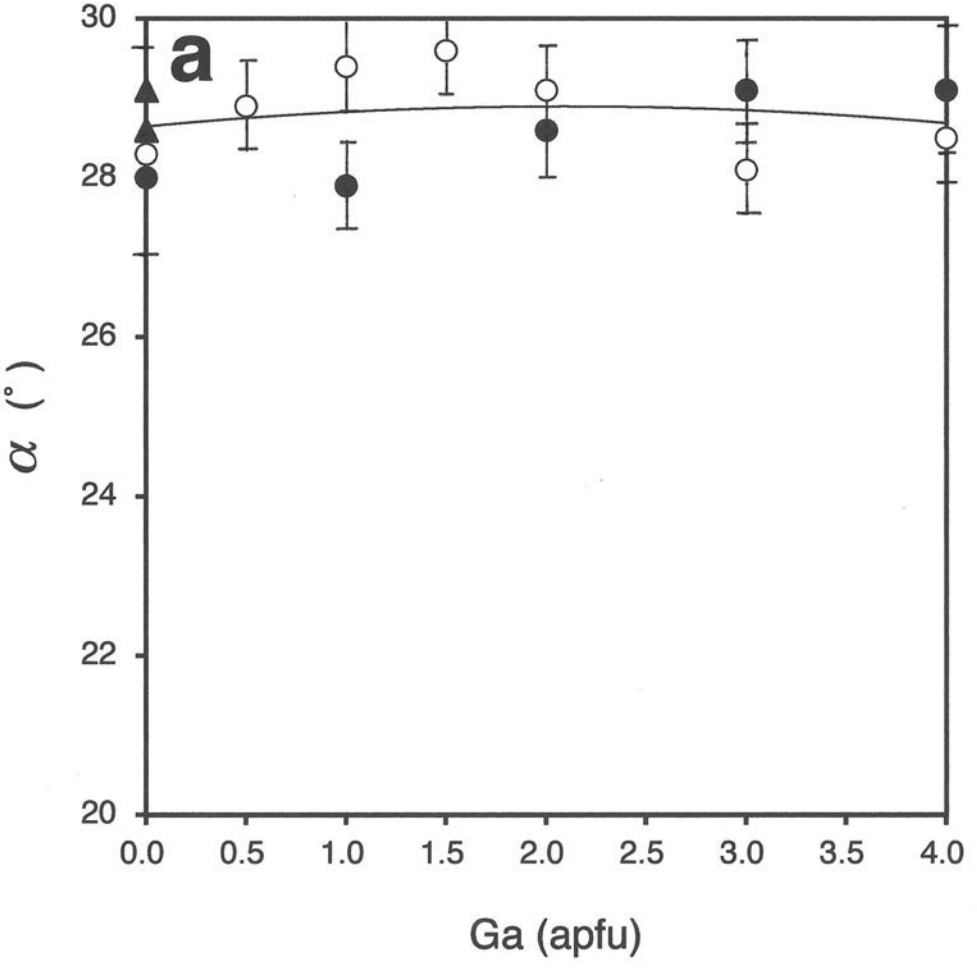

Fig. 7a

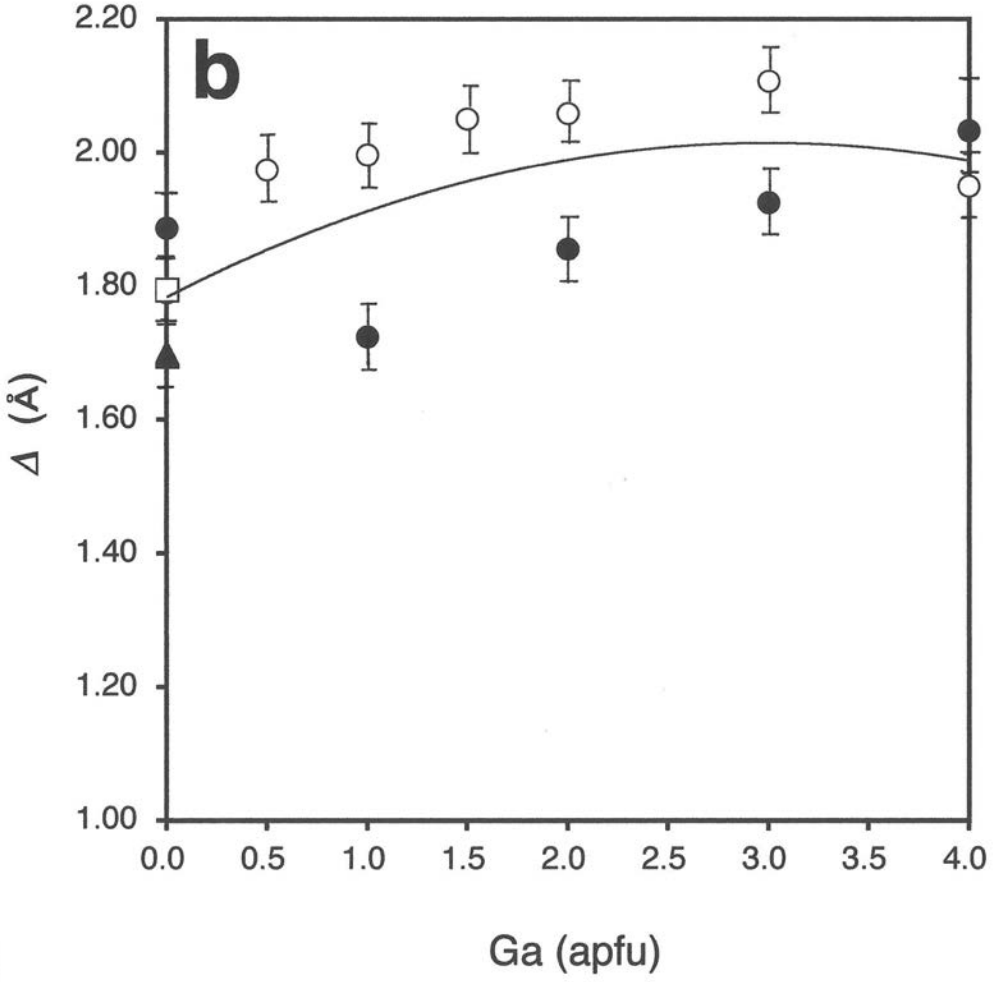

Fig.7b

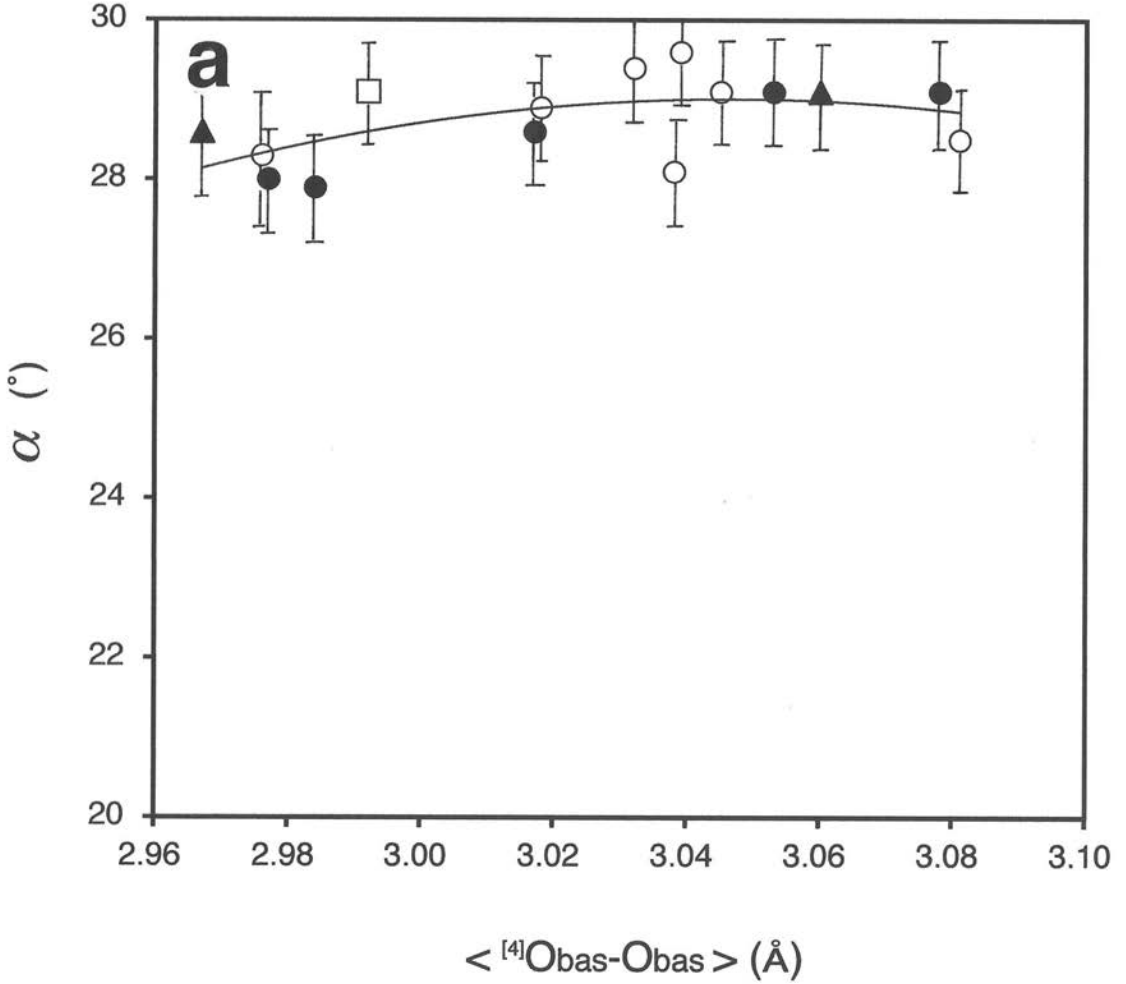

Fig.8a

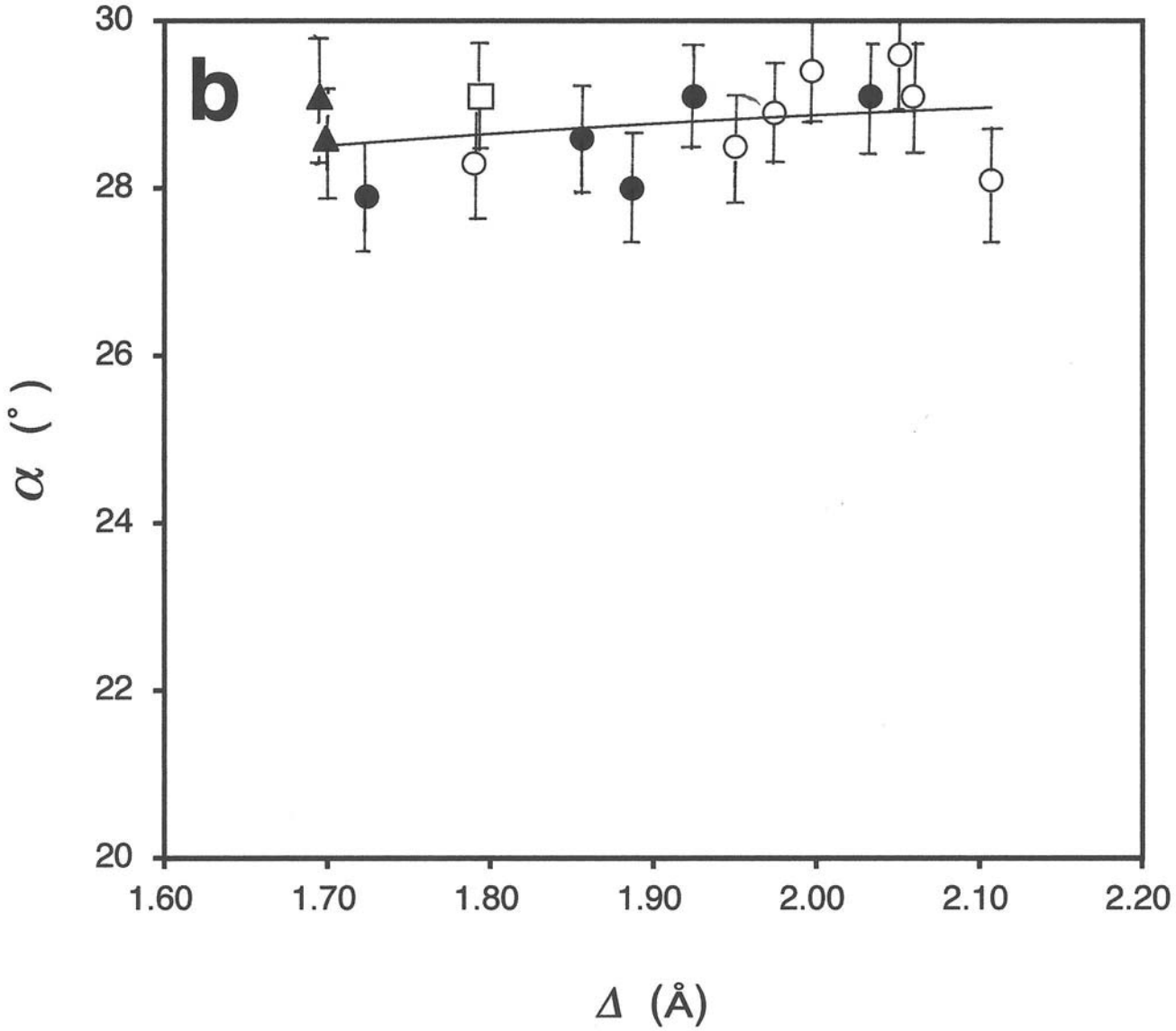

Fig. 8b

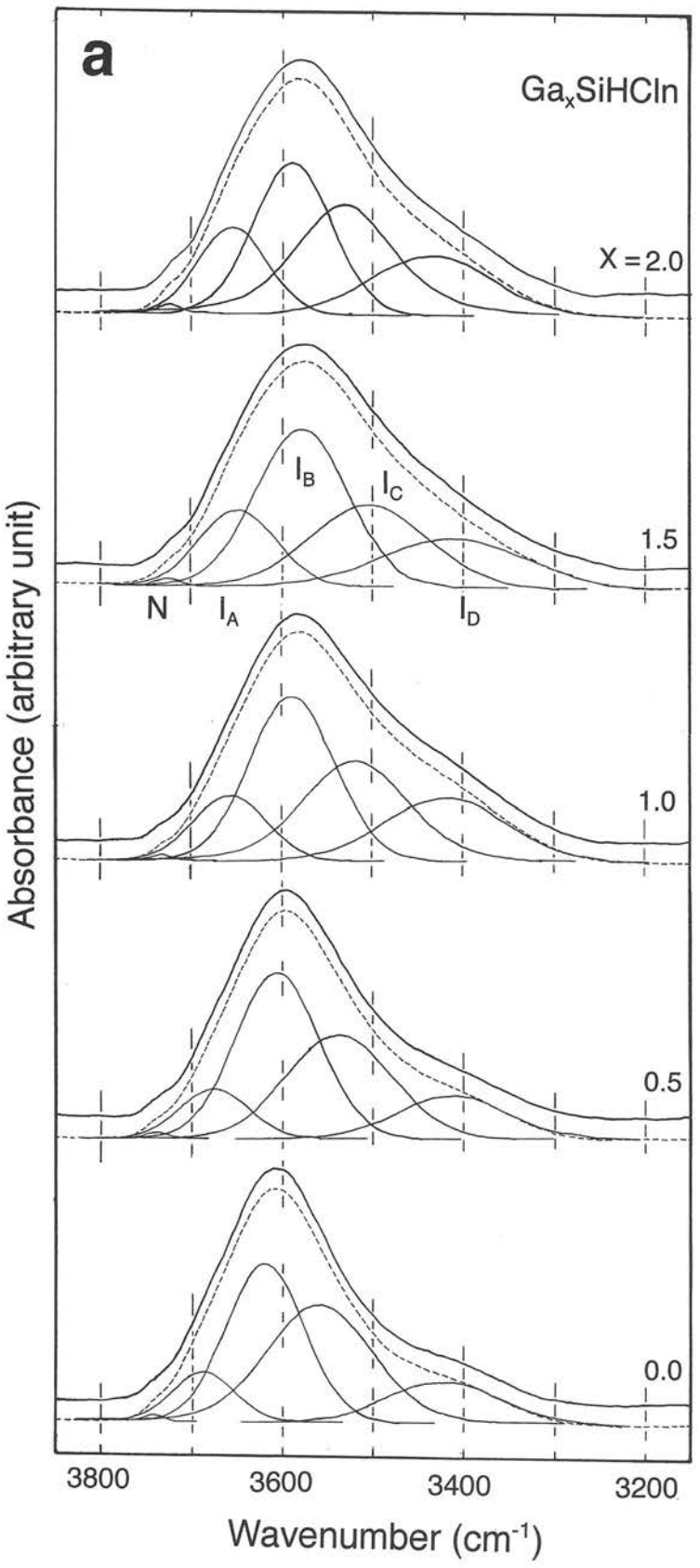
a
Ga$_x$SiHCln
X = 2.0
1.5
1.0
0.5
0.0
I_B
I_C
N
I_A
I_D
Absorbance (arbitrary unit)
3800
3600
3400
3200
Wavenumber (cm^{-1})

Fig. 9a

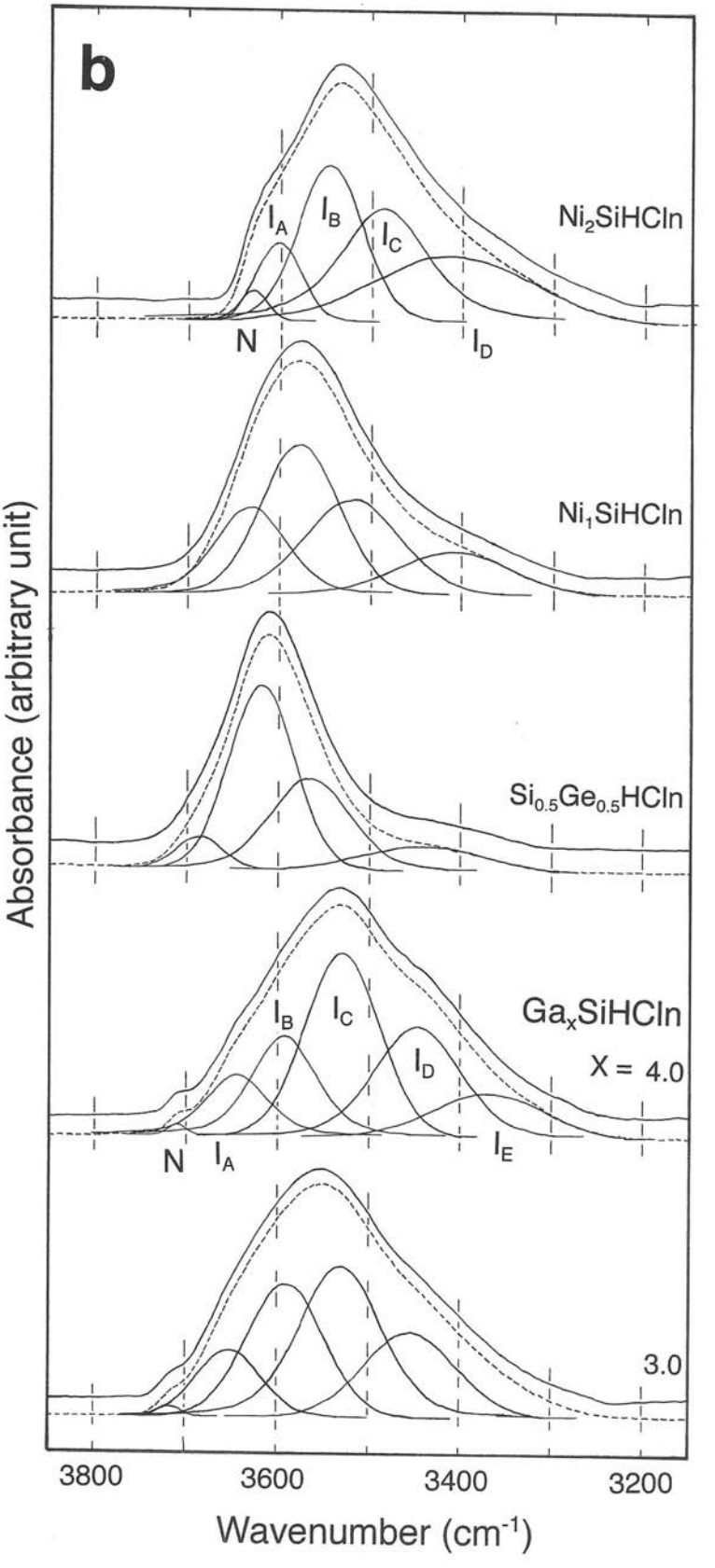
b
Ni2SiHCln
Ni1SiHCln
Si0.5Ge0.5HCln
GaxSiHCln
X = 4.0
3.0
IA
IB
IC
ID
IE
N
Absorbance (arbitrary unit)
3800
3600
3400
3200
Wavenumber (cm-1)

Fig.9b

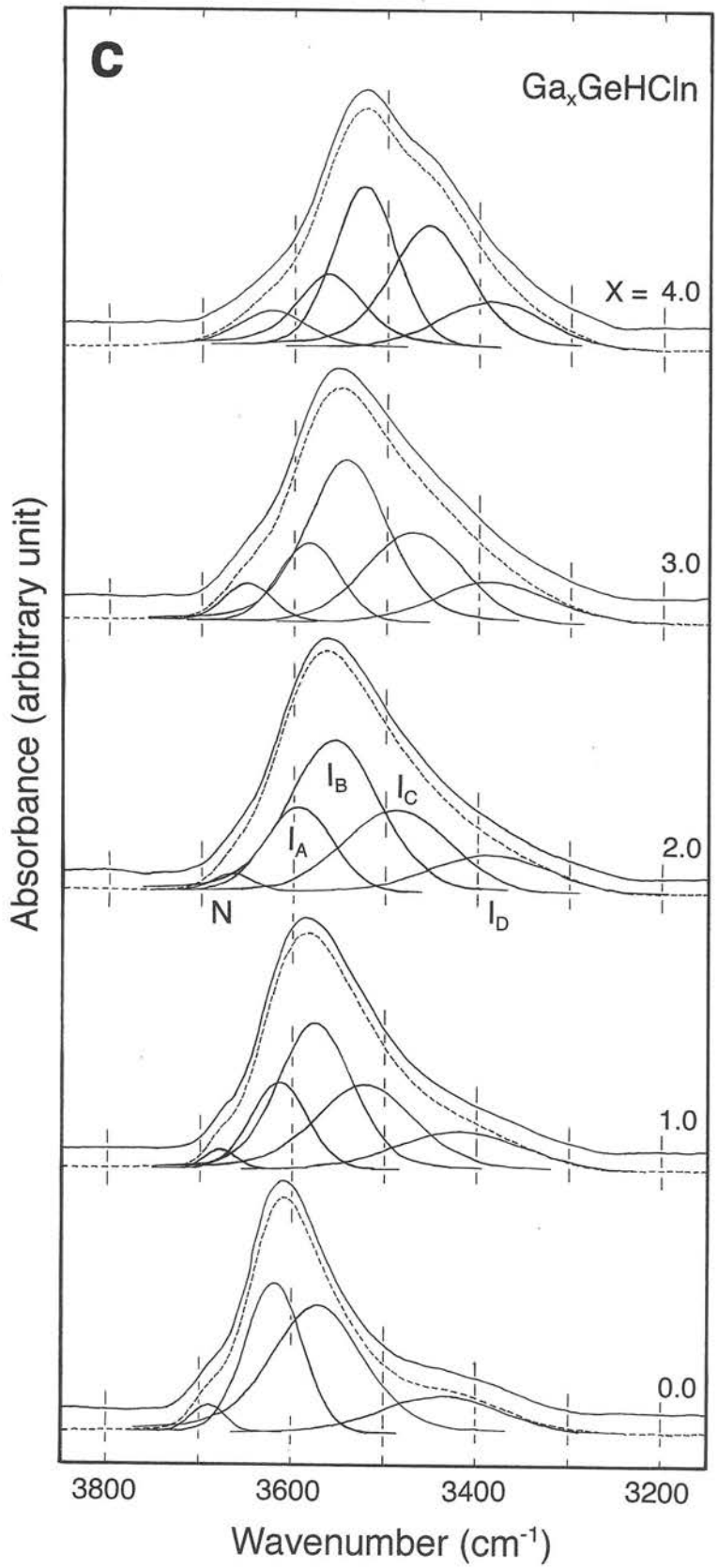
c
Ga$_x$GeHCln
X = 4.0
3.0
2.0
1.0
0.0
I$_A$
I$_B$
I$_C$
I$_D$
N
Absorbance (arbitrary unit)
3800
3600
3400
3200
Wavenumber (cm^{-1})

Fig.9C

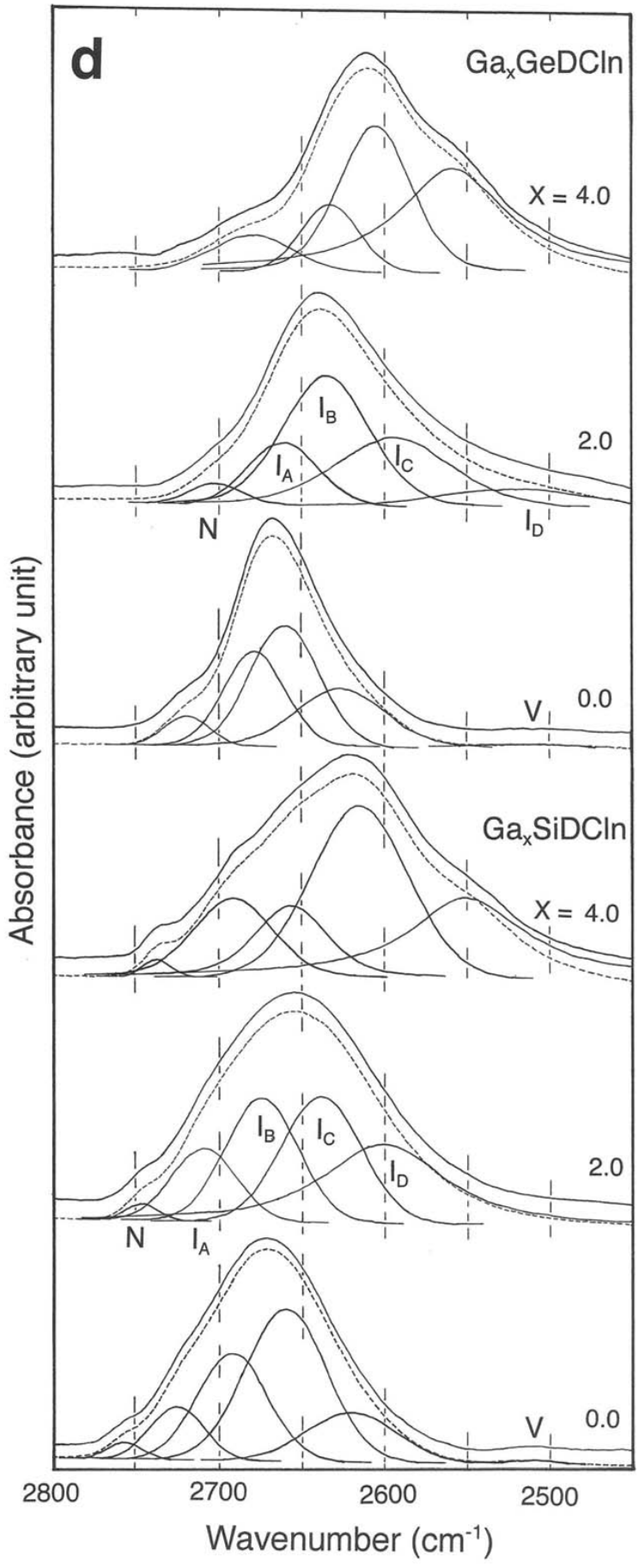
d
Ga$_x$GeDCln
X = 4.0
2.0
I$_B$
I$_A$
I$_C$
I$_D$
N
V
0.0
Ga$_x$SiDCln
X = 4.0
2.0
I$_B$
I$_C$
I$_D$
N
I$_A$
V
0.0
Absorbance (arbitrary unit)
2800
2700
2600
2500
Wavenumber (cm^{-1})

Fig. 9d

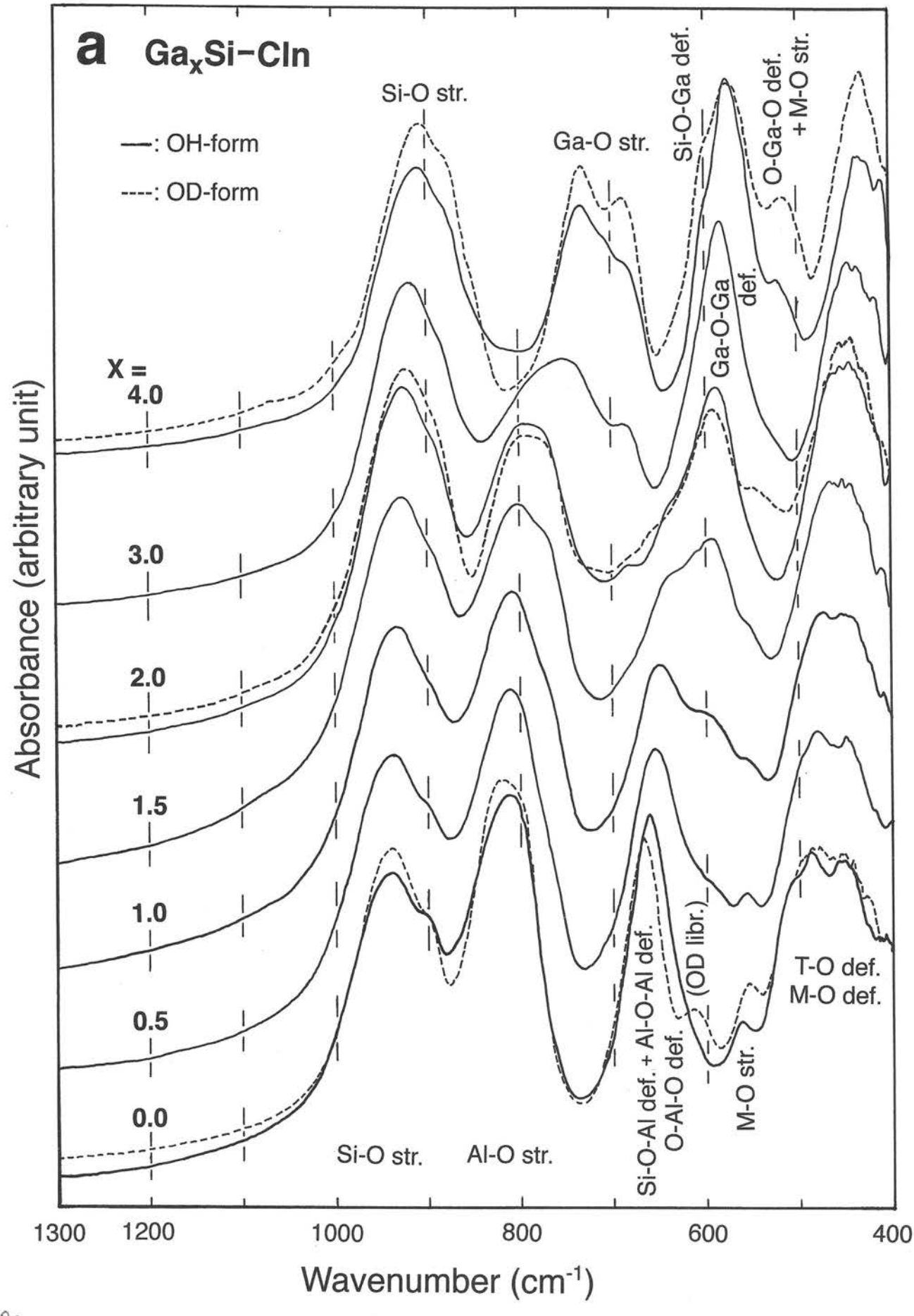
a
Ga_xSi−Cln
—: OH-form
----: OD-form
X =
4.0
3.0
2.0
1.5
1.0
0.5
0.0
Si-O str.
Ga-O str.
Si-O-Ga def.
O-Ga-O def.
+ M-O str.
Ga-O-Ga def.
Si-O str.
Al-O str.
Si-O-Al def. + Al-O-Al def.
O-Al-O def.
(OD libr.)
M-O str.
T-O def.
M-O def.
Absorbance (arbitrary unit)
1300
1200
1000
800
600
400
Wavenumber (cm^{-1})

Fig. 10 a

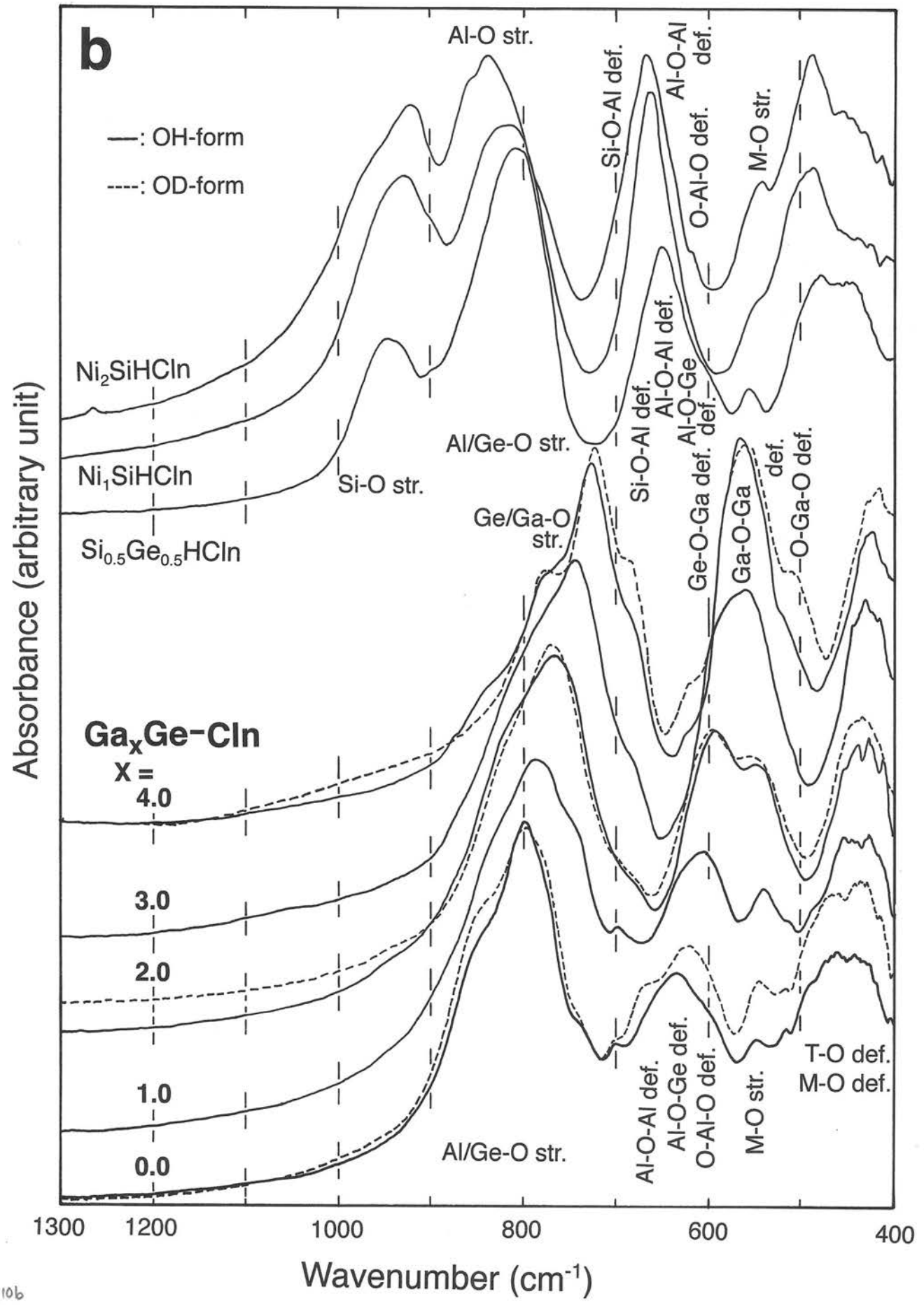
b
—: OH-form
----: OD-form
Al-O str.
Si-O-Al def.
Al-O-Al def.
O-Al-O def.
M-O str.
Ni2SiHCln
Ni1SiHCln
Si0.5Ge0.5HCln
Si-O str.
Al/Ge-O str.
Si-O-Al def.
Al-O-Al def.
Al-O-Ge def.
Ge-O-Ga def.
Ge/Ga-O str.
Ga-O-Ga def.
O-Ga-O def.
GaxGe-Cln
X =
4.0
3.0
2.0
1.0
0.0
Al-O-Al def.
Al-O-Ge def.
O-Al-O def.
M-O str.
T-O def.
M-O def.
Al/Ge-O str.
Absorbance (arbitrary unit)
1300
1200
1000
800
600
400
Wavenumber (cm-1)

Fig. 10b

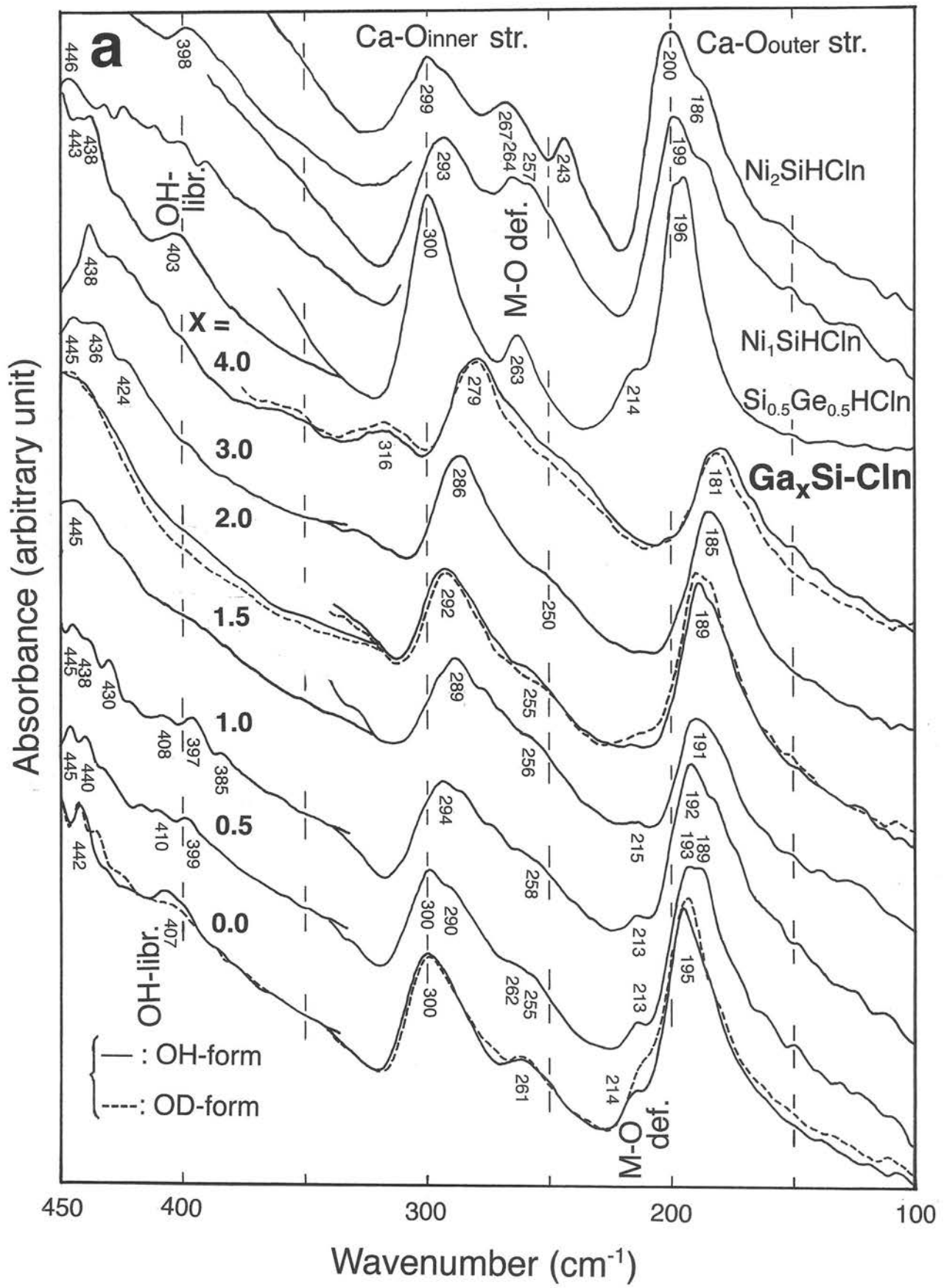
a
Ca-Oinner str.
Ca-Oouter str.
Ni2SiHCln
Ni1SiHCln
Si0.5Ge0.5HCln
GaxSi-Cln
X =
4.0
3.0
2.0
1.5
1.0
0.5
0.0
OH-libr.
M-O def.
OH-libr.
M-O def.
— : OH-form
----: OD-form
Absorbance (arbitrary unit)
Wavenumber (cm-1)
450
400
300
200
100

Fig.11a

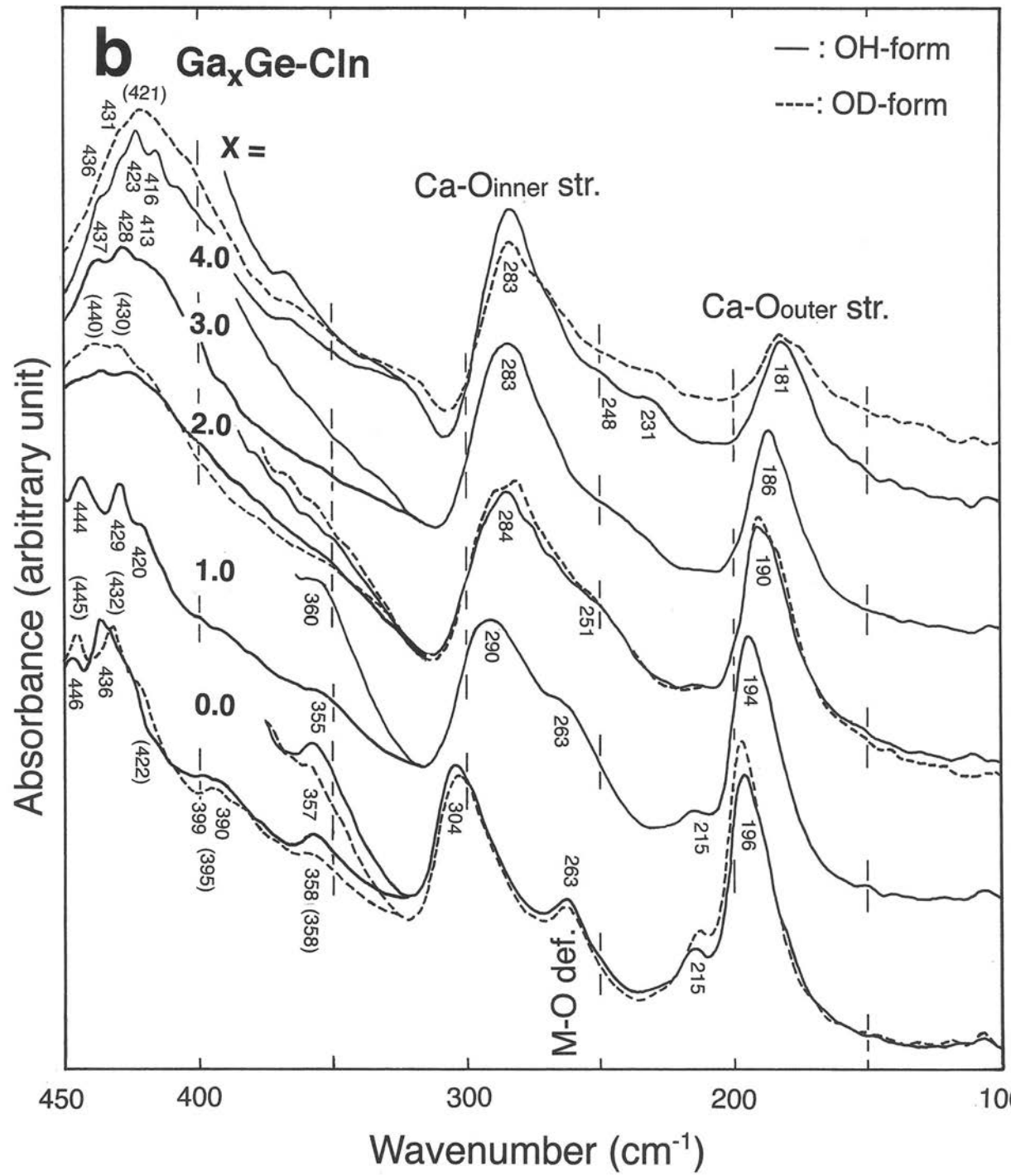
b
Ga$_x$Ge-Cln
— : OH-form
----: OD-form
X =
4.0
3.0
2.0
1.0
0.0
Ca-Oinner str.
Ca-Oouter str.
M-O def.
Absorbance (arbitrary unit)
Wavenumber (cm^{-1})
450
400
300
200
100
(421)
431
436
423
416
428
413
437
(430)
(440)
444
429
420
(445)
(432)
436
446
(422)
399
390
(395)
360
355
357
358 (358)
283
248
231
284
251
290
263
304
263
215
181
186
190
194
196
215

Fig. 11b

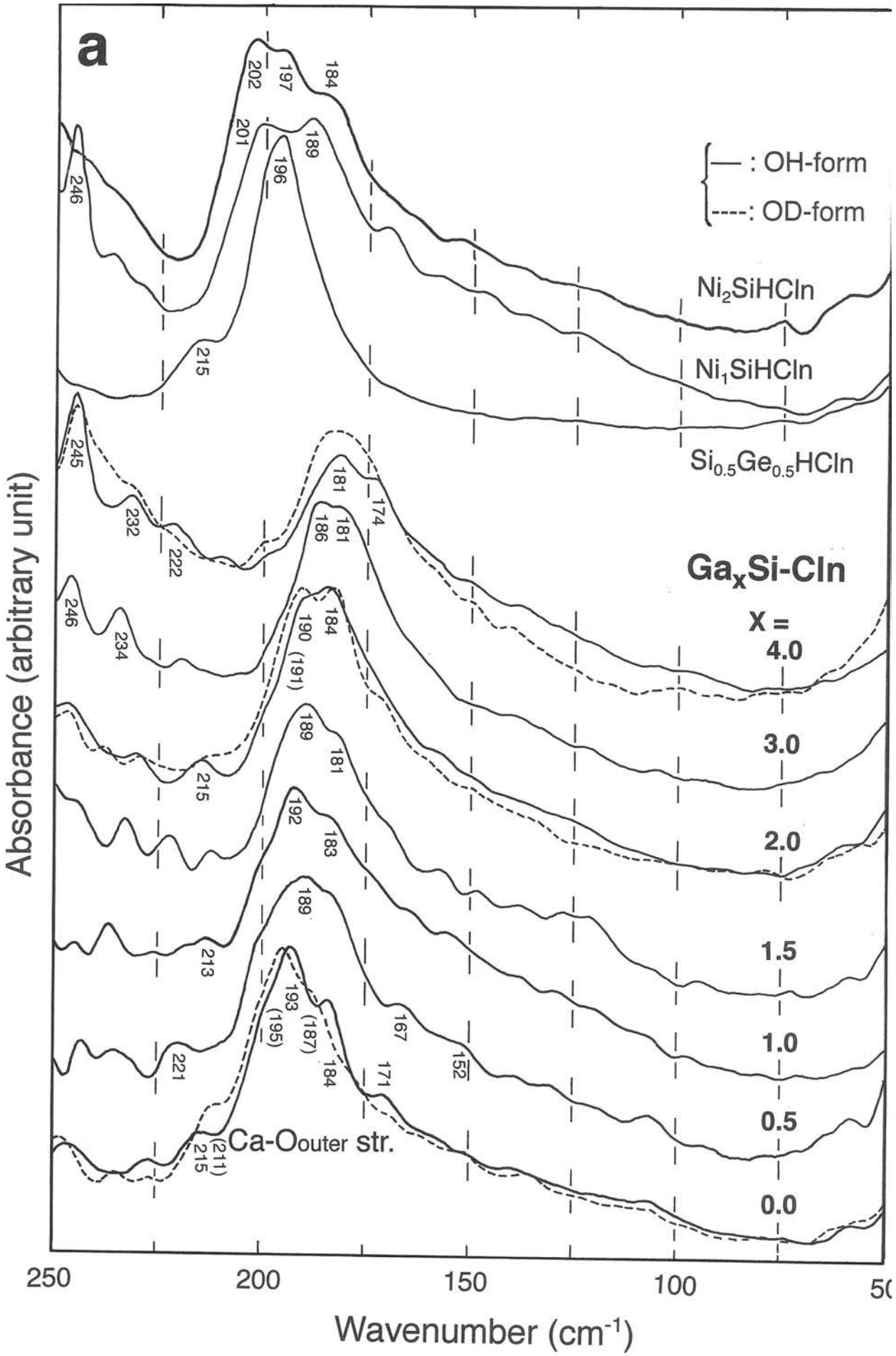
a
— : OH-form
----: OD-form
Ni2SiHCln
Ni1SiHCln
Si0.5Ge0.5HCln
GaxSi-Cln
X =
4.0
3.0
2.0
1.5
1.0
0.5
0.0
Ca-Oouter str.
Absorbance (arbitrary unit)
Wavenumber (cm-1)
250
200
150
100
50

Fig.12a

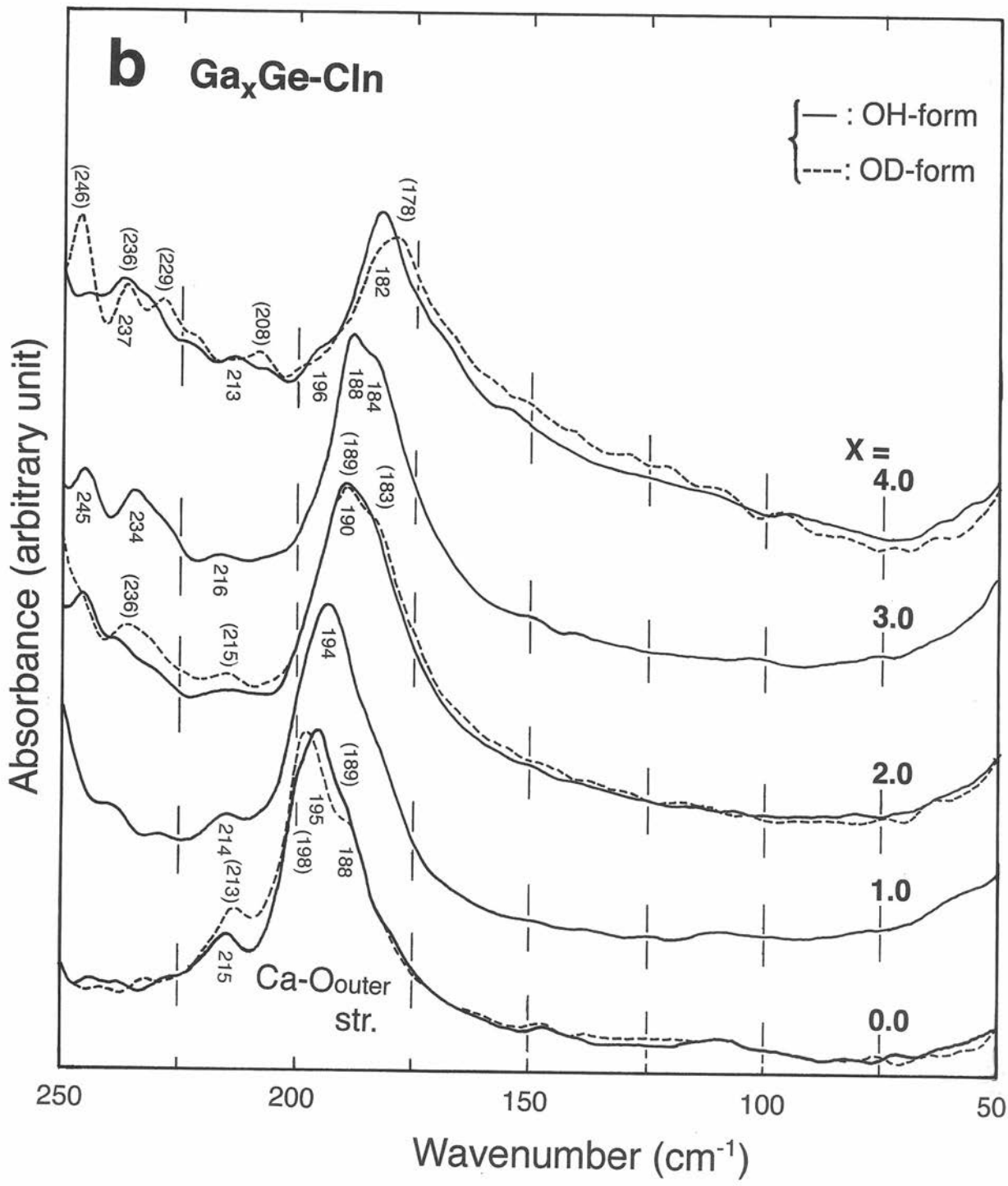
b
Ga$_x$Ge-Cln
— : OH-form
----: OD-form
X =
4.0
3.0
2.0
1.0
0.0
(246)
(236)
(229)
237
213
(208)
196
182
(178)
188
184
(189)
(183)
245
234
216
190
(236)
(215)
194
214
(213)
195
(198)
(189)
188
215
Ca-O$_{outer}$ str.
Absorbance (arbitrary unit)
250
200
150
100
50
Wavenumber (cm^{-1})

Fig. 12b

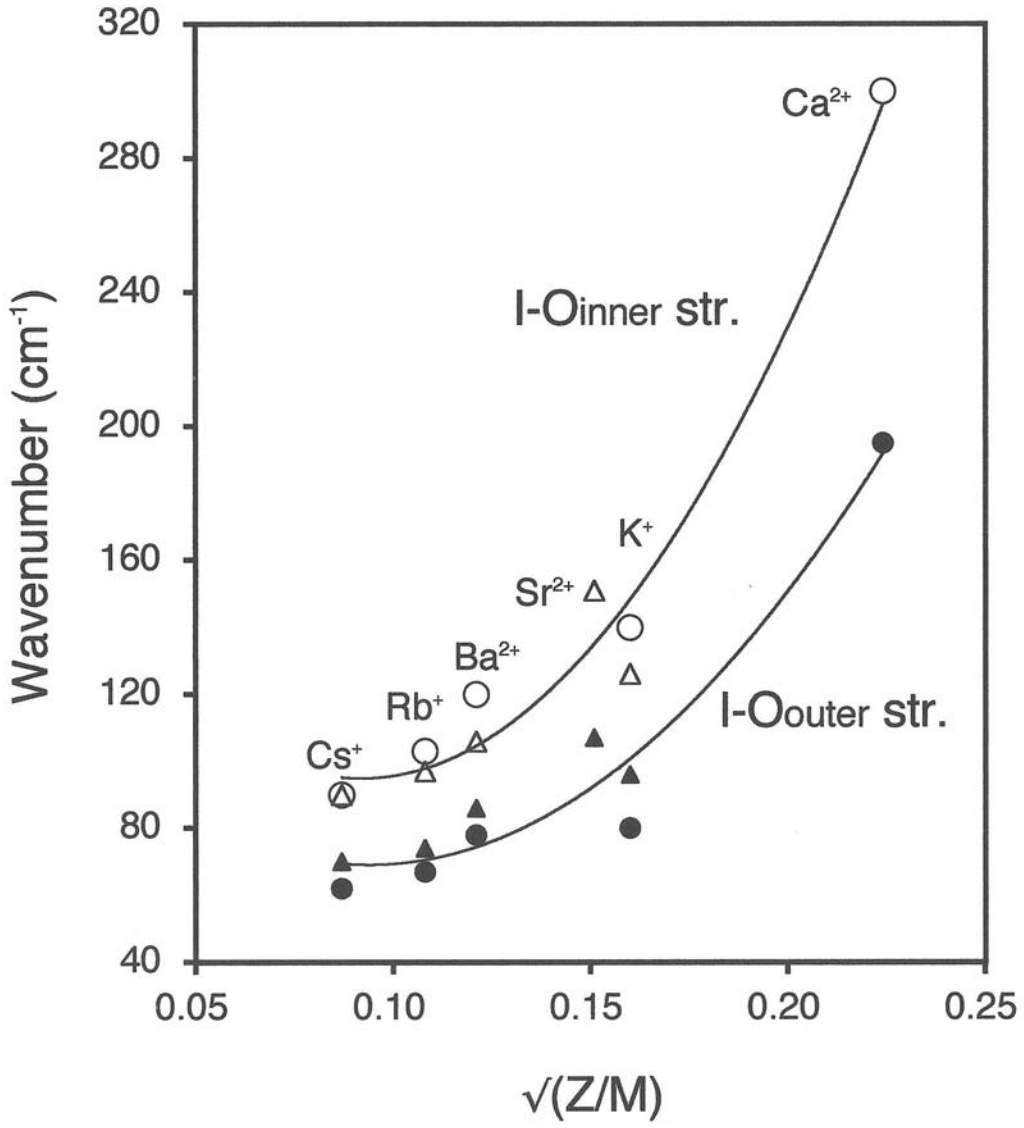
320
280
240
200
160
120
80
40
Wavenumber (cm-1)
0.05
0.10
0.15
0.20
0.25
√(Z/M)
Ca2+
I-Oinner str.
K+
Sr2+
Ba2+
Rb+
Cs+
I-Oouter str.

Fig.14

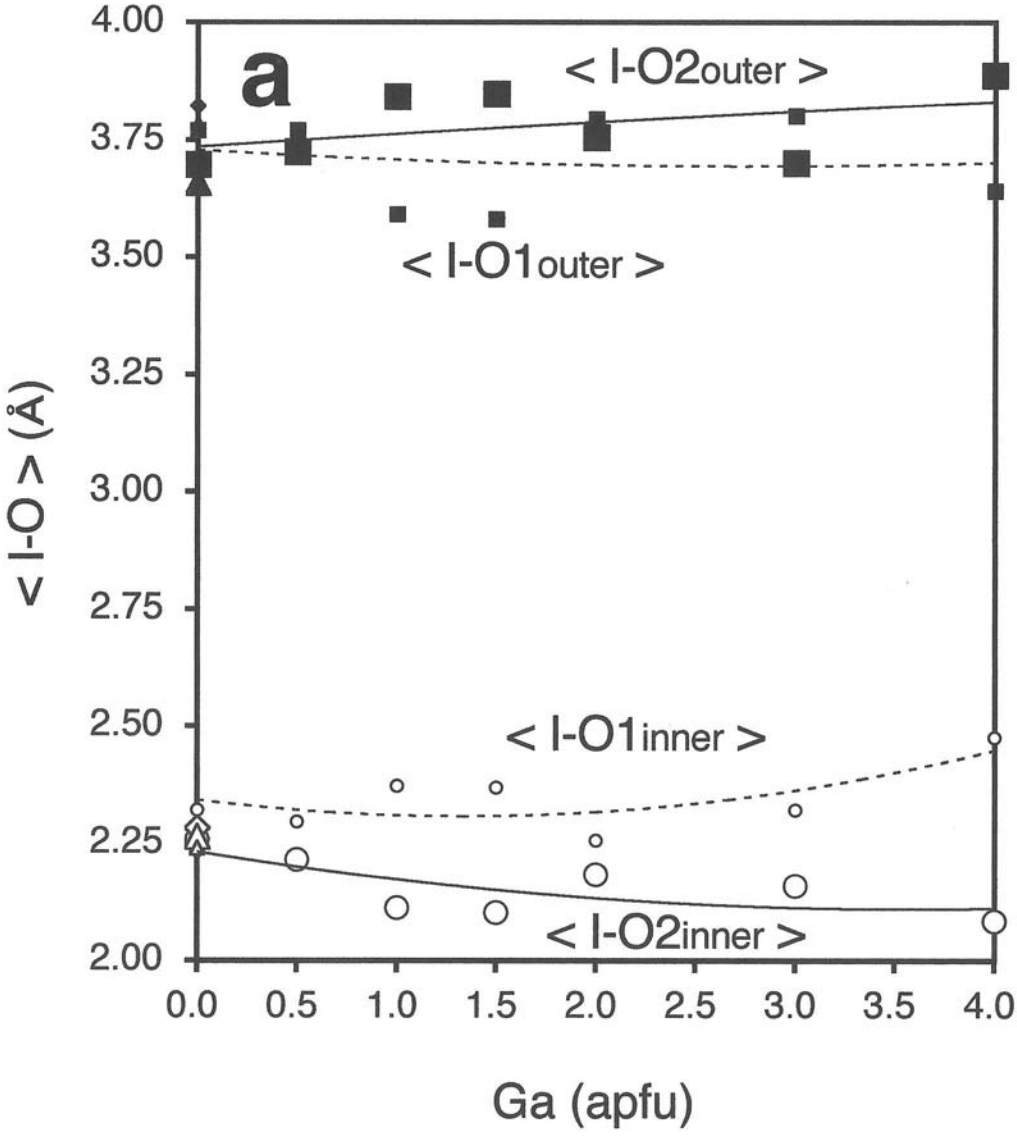
a
< I-O2outer >
< I-O1outer >
< I-O1inner >
< I-O2inner >
< I-O > (Å)
4.00
3.75
3.50
3.25
3.00
2.75
2.50
2.25
2.00
0.0
0.5
1.0
1.5
2.0
2.5
3.0
3.5
4.0
Ga (apfu)

Fig.15a

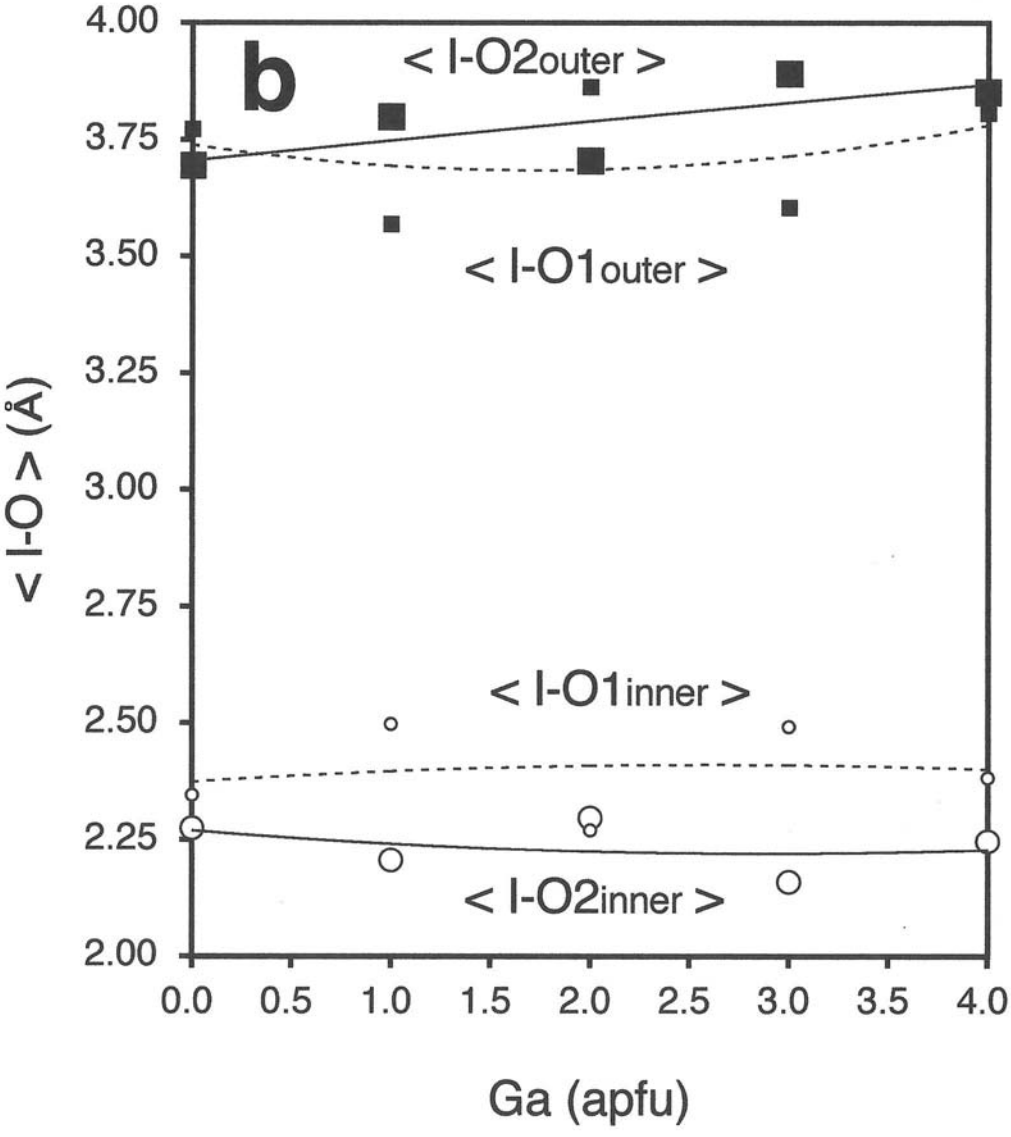
b
< I-O2outer >
< I-O1outer >
< I-O1inner >
< I-O2inner >
< I-O > (Å)
Ga (apfu)
4.00
3.75
3.50
3.25
3.00
2.75
2.50
2.25
2.00
0.0
0.5
1.0
1.5
2.0
2.5
3.0
3.5
4.0

Fig. 15b